

AD 654450

APL/JHU CF- 2813

March 1959

Copy No. 64

AN APPROXIMATE ANALYSIS OF THE TWO-DIMENSIONAL,
SUPERSONIC FLOW PAST A PLANE WALL WITH SUPER-CRITICAL
HEAT ADDITION IN A NORMAL PLANE

by

Henry W. Woolard

The CF series of papers is intended to be a flexible means for the reporting of preliminary investigations, or subject matter of limited interest. The information presented herein may be tentative, and subject to modification. This paper may not be reproduced except with the express permission of the issuing agency.

Initial distribution of this document is confined to persons and organizations within Section T immediately concerned with the subject matter. Upon special request, copies of this report may be made available to other organizations having a stated need for the information presented.

THE JOHNS HOPKINS UNIVERSITY
APPLIED PHYSICS LABORATORY
Silver Spring, Maryland

Operating under Contract NOrd 7386 with the Bureau of Ordnance, Department of the Navy

DDC
JUL 11 1957
E

THIS DOCUMENT HAS BEEN APPROVED
FOR PUBLIC RELEASE AND SALE: ITS
DISTRIBUTION IS UNLIMITED

ARCHIVE COPY

APPLIED PHYSICS LABORATORY
THE JOHNS HOPKINS UNIVERSITY
SILVER SPRING MARYLAND

AN APPROXIMATE ANALYSIS OF THE TWO-DIMENSIONAL,
SUPERSONIC FLOW PAST A PLANE WALL WITH SUPER-CRITICAL
HEAT ADDITION IN A NORMAL PLANE

by

Henry W. Woolard

March 1959

SUMMARY

An analysis is performed to determine approximately the flow field and the normal forces acting for the two-dimensional, supersonic, zero angle-of-attack flow about a flat plate with super-critical heat addition (i.e., with thermal choking downstream) at a normal finite-height heater plane on one side of the flat plate. The results of the analysis have possible application to the design of an external thrust and/or lift producing device for airborne supersonic vehicles.

Charts for the determination of the pertinent flow-field parameters and the normal force coefficients as a function of the rate of heat addition and free-stream Mach number, are presented for Mach numbers ranging from 2.0 to 7.0.

PRINCIPAL SYMBOLS

a	speed of sound
\bar{a}	mean speed of sound on the sonic line $\overline{\rho_1 \rho_2}$ (See Fig. 1)
A	cross-sectional area of a stream tube
A_*	cross-sectional area of a stream tube at $M = 1.0$
b	parameter defined by Eq. (2)
B	$= (P_0/\bar{P}) (A/A_*)_0$
c_p	specific heat at constant pressure
C	$= \beta (\beta \tan \varphi_{\rho_1} - \sqrt{\beta^2 \tan^2 \varphi_{\rho_1} - 1})$
C_p	pressure coefficient, $(p-p_0)/q_0$
h_0	free-stream capture height (See Fig. 1)
h_2, h_3	height of the heater (See Fig. 1)
h_0^*	non-dimensional capture height, h_0/h_2
$1 - h_0^*$	spillage
$(1 - h_0^*)_{\rho_1}$	spillage corresponding to the case where the mass flow across the sonic line is equal to the mass flow through the heater
L	shock standoff distance (See Fig. 1)
L^*	L/h_2
\mathcal{M}	moment
M	local Mach number
M_0	free stream Mach number
\bar{M}	mean Mach number just upstream of the second shock wave
p	static pressure
\bar{p}	mean static pressure on the sonic line $\overline{\rho_1 \rho_2}$ (See Fig. 1)
$\underline{\underline{p}}$	static pressure corresponding to \bar{M} and \bar{P}

p_{10}	local wall-static pressure along $\overline{x_0x_2}$ (See Fig. 1)
p_{11}	local wall-static pressure downstream of x_3 (See Fig. 1)
\tilde{p}_{11}	local wall-static pressure downstream of x_3 for a simply reflected Prandtl-Meyer expansion (See text)
\tilde{p}_∞	\tilde{p}_{11} at $x = \infty$
P	total pressure
\bar{P}	total pressure downstream of the first shock wave and along the mean streamline having the free-stream ordinate \bar{y}
$\overline{\bar{P}}$	total pressure downstream of the first shock wave and along the mean streamline having the free-stream ordinate $\overline{\bar{y}}$
q_0	free-stream dynamic pressure, $\rho_0 U_0^2/2$
q_H	heat flow per unit time per unit area
R	gas constant
T	static temperature
U_0	free-stream velocity
Y	normal force per unit width, parallel to the y-axis, positive in the positive y-direction
Y_{10}	forward normal force per unit width acting on the surface $\overline{x_0x_2}$ in Fig. 1
Y_{11}	aft normal force per unit width acting on the surface $\overline{x_3x}$ in Fig. 1
Y_{11m}	aft normal force per unit width acting on the surface $\overline{x_3x_m}$ in Fig. 1
Y_{11t}	aft normal force per unit width acting on the surface extending from x_3 to x_t
$Y_{11\infty}$	infinite-plate aft normal force per unit width, i.e. the normal force acting on the surface extending from x_3 to infinity
Y_t	$= Y_{10} + Y_{11t}$
Y^*	normal force coefficient, $Y/q_0 h_2$
x, y	rectangular coordinates (See Fig. 1)

- x^*, y^* non-dimensional rectangular coordinates, x/h_2 and y/h_2 respectively
- x_I, y_I coordinates of the intersection of the first and second shock waves
- x_m x-intercept of the unrefracted last Prandtl-Meyer characteristic emanating from the top of the heater
- x_t coordinate at which the cumulative aft normal force equals nine-tenths of infinite-plate aft normal force at zero spillage
- x_{cp} coordinate of the center of pressure of the normal force
- \bar{y} free-stream ordinate of the mean streamline representing all the fluid flowing across the sonic line ρ_1, ρ_2 , $\bar{y} = h_0 + (1/2)(y_{\rho_1} - h_0)$ (See Fig. 1)
- $\bar{\bar{y}}$ free-stream ordinate of the mean streamline used in determining \bar{M} and $\bar{\theta}$, $\bar{\bar{y}} = 3h_0/2$ (See Fig. 1)
- β $= \sqrt{M_0^2 - 1}$
- γ ratio of specific heats, c_p/c_v
- μ Mach angle, $\cot^{-1} \beta = \sin^{-1} (1/M)$
- η angle between sonic line and the normal to the free-stream direction $\eta = \theta_{\rho_1}$
- θ local flow direction measured relative to the x-axis
- θ_{ρ_1} local flow direction downstream of the sonic point on the first shock wave
- $\bar{\theta}$ mean flow direction just upstream of the second shock wave
- $\bar{\theta}_u$ upper limiting value of $\bar{\theta}$, i.e. that value of $\bar{\theta}$ for which second shock wave becomes a Mach wave
- $\bar{\theta}_l$ lower limiting value of $\bar{\theta}$, i.e. that value of $\bar{\theta}$ for which sonic velocity occurs behind the second shock wave
- ν Prandtl-Meyer angle (angle through which a supersonic stream is turned in expanding from $M = 1$ to $M > 1$)
- $\nu + \theta$ characteristic constant for a right-running characteristic

$\gamma - \theta$	characteristic constant for a left-running characteristic
ρ	mass density
$\bar{\rho}$	mean mass density on the sonic line $\bar{\rho}_1 \bar{\rho}_2$ (See Fig. 1)
τ	total temperature
$\Delta\tau$	$= \tau_3 - \tau_0$
ϕ	local shock wave angle for the first shock wave
θ	local shock wave angle for the second shock wave
$\bar{\theta}$	the mean inclination of the second shock wave in the vicinity of the heater. Based on \bar{M} and $\bar{\theta}$, and measured relative to the x-axis
$\bar{\theta}_0$	mean inclination of the second shock wave corresponding to zero flow deflection, i.e. the Mach wave angle corresponding to \bar{M} .
$\bar{\theta}_s$	mean inclination of the second shock wave for the occurrence of sonic velocity aft of the shock
θ	$= (1 + \gamma M^2) M^{-1} \left[2(1 + \gamma) \left(1 + \frac{\gamma - 1}{2} M^2 \right) \right]^{-1/2}$

Subscripts and Superscripts

CR	denotes conditions corresponding to critical heat addition, i.e., that amount of heat addition which just produces sonic velocity downstream of the heater
o	denotes free stream conditions when used as a subscript
m	denotes conditions corresponding to the unrefracted last Prandtl-Meyer characteristic
R	right-running characteristic
L	left-running characteristic
s	denotes conditions at the sonic line
s_1	denotes conditions pertaining to the sonic point on the detached shock
t	denotes conditions corresponding to the aft normal force Y_{11_t} (See Y_{11_t})
u, l	denotes conditions corresponding respectively to the upper and lower limiting values of $\bar{\theta}$ (See $\bar{\theta}$)

- 1,2,3,
etc. denotes conditions at the corresponding stations shown in Fig. 1
- ν denotes conditions corresponding to a Prandtl-Meyer expansion from sonic velocity through the angle ν
- denotes mean conditions on the sonic line $\overline{\rho_1 \rho_2}$, except when used with \bar{y}
- = denotes mean conditions just upstream of the second shock, except when used with \bar{y} and $\bar{\Phi}$
- \sim denotes quantities associated with a simply reflected Prandtl-Meyer expansion
- * denotes a non-dimensional quantity when used as a superscript. Forces are made non-dimensional by dividing by $q_0 h_2$. Lengths are made non-dimensional by dividing by h_2
- * denotes sonic conditions when used as a subscript

INTRODUCTION

In the ever present effort to improve the over-all operational and performance capabilities of supersonic airborne vehicles, consideration has been given recently to the possibility of obtaining thrust and/or lift by the addition of heat to the external flow about a vehicle. Conceivably, the heat is added either by external combustion or by an external heat exchanger. A comprehensive, although not complete, list of unclassified publications dealing with various facets of the subject of heat addition to a flowing fluid is presented herein as Refs. 1 through 24)¹. Most of these publications are concerned with the basic flow field problem, usually, except for Refs. 21 through 24, without detailed consideration of the mechanics of the heat addition process itself. Investigations comparing the efficiency of lift or thrust production of a vehicle with external heat addition with a conventional ramjet--or turbojet--powered vehicle are reported by Pinkel, Serafini, and Gregg in Ref. 17, Gazley in Ref. 18, Mager in Ref. 19, and Willmarth in Ref. 20. Briefly, these later investigations conclude that the efficiency of the external heat addition system is roughly of the same order as the more conventional arrangements for small amounts of heat addition. This, coupled with the difficulties of adding heat externally, presents a rather pessimistic picture for the external system. Although, on the basis of the foregoing investigations, the external arrangement appears to have no advantage or at the most only a marginal advantage over the internal system in its thrust and/or lift producing

¹References may be found on pages 36-39.

efficiency, it is felt that it should not be abandoned since other advantages possibly can be realized, such as, for example, a more compact vehicle or a reduction of cooling and structural requirements.

Except for the treatments of one-dimensional flow (Refs. 1, 2, 3, 4, and 5), the explicit solutions obtained in Refs. 1 through 19 for supersonic flow are for small amounts of heat addition. Willmarth (Ref. 20) treats the case of a large amount of heat addition on a flat plate wherein the heat addition region is the shape of a semi-infinite wedge and produces a semi-infinite oblique shock.

The present paper is concerned with the approximate analysis of the flow field, and hence the determination of the normal forces, for two-dimensional, supersonic, zero angle-of-attack flow about a flat plate with super-critical heat addition² at a finite-height normal plane (the heater) on one side of the flat plate (see Fig. 1). Such a situation would occur, for example, for plane heat addition on the double wedge airfoils shown in Fig. 2. The detailed mechanism of the heat addition process is not considered. Nor is any consideration given to the determination of the forces acting on appendages, such as flame holders, or heat exchangers which might be required in the heat addition process. Although the replacement of a combustion region or a heat exchanger by a heater plane greatly oversimplifies the real situation, it does serve to establish the order of magnitude of the normal forces. The present analysis represents an advance over previous work in that it treats large amounts of heat added over a region of finite extent in the normal direction.

²Critical heat addition is defined as that amount of heat addition which just produces sonic velocity downstream of the region of heat addition.

For the model analyzed, generalized charts showing the pertinent flow quantities and normal-force coefficients as a function of free stream Mach number and heat addition have been prepared for an ideal gas with a constant gamma of 7/5, and for Mach numbers ranging from 2.0 to 7.0. Generally, the gamma associated with heat addition will be different from 7/5 due to the presence of combustion gases or to real-gas effects associated with high stagnation temperatures, or both. Refinements taking into account these effects have not been included in this paper, since the primary purpose is to determine gross effects, and because their inclusion seems unwarranted in view of the numerous approximations which have been made.

DESCRIPTION OF THE MATHEMATICAL MODEL

In this section a general description of the mathematical model employed in the analysis is given for the purpose of orienting the reader with respect to the detailed discussions and analyses presented in subsequent sections.

Figure 1 depicts approximately the flow pattern for super-critical heat addition. For sub-critical heat addition there is no spillage of the flow over the top of the heater, and hence, for this regime the first shock wave shown in the figure does not exist.³ The gross flow characteristics for the flow between the x-axis and the streamline $\overline{DA\mathcal{A}_2}$ are calculated on the basis of a one-dimensional stream tube whose

³At critical heat addition we will continue to call the shock wave emanating from the top of heat addition region the "second shock wave" even though there no longer exists a first shock wave.

area varies from h_0 to h_2 and for which heat addition has taken place at constant area, i.e. $h_2 = h_3$. The dimensions h_0 , h_2 , and L , must of course be compatible with the continuity requirements resulting from heat addition, and with the first shock wave configuration.

The first shock wave configuration is determined by considering the heater to behave like a supersonic inlet and by utilizing the continuity method, developed by Moeckel in Ref. 25, for approximately predicting the form and location of a detached shock wave ahead of an inlet.

In the Moeckel analysis, the shape of the detached shock along AH in Fig. 1 is assumed to be a hyperbola with a Mach line as an asymptote. The location x_0 of the vertex A is dependent upon the inclination and length of the hypothetical sonic line $\overline{A_1 A_2}$. Moeckel assumes that the inclination η of the sonic line is equal to the flow inclination θ_{A_1} , downstream of the sonic point A_1 on the detached shock wave. For a specified spillage, $1 - h_0^*$, the length of the sonic line is determined from the continuity relation through the use of a mean sonic velocity \bar{a} which is assumed to be normal to the sonic line. The magnitude of the mean sonic velocity is that which would exist on a streamline representing the mass centroid of the fluid flowing across the sonic line $\overline{A_1 A_2}$ in Fig. 1. The ordinate of this streamline prior to its passage through the shock wave is given by $\bar{y} = 1/2(y_{A_1} - h_0) + h_0$.

Downstream of the heater the flow executes a Prandtl-Meyer expansion with right-running characteristics centered at the point G in Fig. 1. The boundary conditions at the interface require that the pressure and flow directions on opposite sides of the interface be equal. There is, however, a discontinuity in velocity, total temperature, and total pressure across the interface. For any given set of conditions,

there exists, as we progress downstream from the heater, a last curved right-running Prandtl-Meyer characteristic, $\gamma_m + \theta_m$, corresponding to the boundary conditions at G. The curvature of this characteristics is due to refractions caused by its intersection with upstream wall-reflected Prandtl-Meyer characteristics (not shown in the figure). All right-running characteristics downstream of the last Prandtl-Meyer characteristic are characteristics which have been partially reflected from the interface.

For reasons which will soon be apparent, the last right-running Prandtl-Meyer characteristic is shown in Fig. 1 as a straight line, that is, unrefracted. The intersection of the unrefracted last Prandtl-Meyer characteristic with the x-axis is denoted by x_m^* . This intercept is given by

$$x_m^* - x_3^* = \cot^{-1} (\mu_4 - \theta_4)$$

An approximate method of determining the wall pressure distribution downstream of the heater is developed on the basis of observations made from method of characteristics calculations for critical heat addition at $M_0 = 2.0$ and $M_0 = 6.0$. The details are given in the section entitled "The Downstream Pressure Distribution". It was observed, from these calculations, that the major portion of the pressure drop along the plate occurs in the region between x_3^* and x_m^* , and that the drop in pressure along the plate from x_m^* to $x^* = \infty$ occurs at a rather slow spacewise rate. This behavior of the downstream flow also manifests itself in a very gradual downstream attenuation of the second shock wave. It was further observed that the intersection of a wall-reflected Prandtl-Meyer characteristic with a right-running Prandtl-Meyer characteristic farther downstream refracted the downstream characteristic only slightly. Consequently, to a very good approximation, the pressure distribution in the

region $x_3^* \leq x^* \leq x_m^*$ can be taken as that occurring for the reflection of unrefracted straight-line right-running Prandtl-Meyer characteristics at the wall. This will be referred to hereafter as a simply reflected Prandtl-Meyer expansion. In view of the rather gradual downstream interaction of the shock wave and the heated wake observed in the foregoing method of characteristics calculations, it appears appropriate to approximate the pressure distribution downstream of x_m^* by a two-parameter descending exponential variation with x^* . Some limitations on this approximation are discussed in the section dealing with the details of the downstream pressure distribution.

In applying the approximate method to super-critical heat-addition flow, the mean inclination of the curved second shock wave in the vicinity of the heater top is approximately represented by a straight shock wave whose strength and inclination are dependent upon a mean Mach number \bar{M} and a mean flow direction $\bar{\theta}$ just upstream, and upon the boundary conditions at the interface. The methods of determining these mean values are described in detail in a subsequent section.

ONE-DIMENSIONAL HEAT ADDITION RELATIONS

The governing relations for heat addition in one-dimensional flow have been reported upon and discussed many places in the literature and are now rather familiar to most engineers and scientists. (See, e.g., Refs. 1, 2, 3, 4, and 5.) For this reason the presentation in this section is principally concerned with the final relations pertinent to the analysis.

With reference to Fig. 3, consider a flow with heat addition in a variable area duct with a constant upstream supersonic Mach number, M_0 . This situation is analogous to the flow between the streamline $DA\bar{A}_2$ and the x-axis in Fig. 1. In the arrangement shown in Fig. 3, heat is added at station II. The area at station II is held constant, while that at station I is adjustable to the flow-continuity requirement. The length " l " is completely arbitrary. For flow with sub-critical heat addition, the area ratio h_0/h_3 is equal to unity, the Mach number M_3 is less than M_0 , and there is no shock wave present. At critical heat addition, the area ratio h_0/h_3 continues to remain at unity, the Mach number M_3 is unity (thermal choking), and a normal shock wave is on the verge of appearing. For flows with super-critical heat addition, the area ratio h_0/h_3 is less than unity at values consistent with the continuity requirement, the Mach number M_3 remains at a constant value of unity, and the normal shock establishes itself in the upstream duct having the height h_0 .

In this paper we are concerned with flows having critical and supercritical heat addition. For this regime, the applicable relations are presented below. These relations are available, in perhaps slightly different form, in a variety of places in the previously cited literature.

For critical and super-critical heat addition:

$$\frac{\tau_3}{\tau_0} = \frac{\tau_3}{\tau_2} = \left(\frac{\gamma_3 R_2}{\gamma_2 R_3} \right) \left(\frac{1 + \gamma_2}{1 + \gamma_3} \right) \theta^2 (M_2)$$

$$\theta(M_2) = \frac{(1 + \gamma_2 M_2^2) M_2^{-1}}{\sqrt{(1 + \gamma_2) [2 + (\gamma_2 - 1) M_2^2]}} = \frac{(1 + \gamma_2 M_2^2) \sqrt{(T/\tau)_2}}{M_2 \sqrt{2(1 + \gamma_2)}}$$

$$\frac{P_3}{P_0} = \frac{\left(\frac{1 + \gamma_3}{2}\right)^{\frac{1}{\gamma_3 - 1}}}{\left(\frac{1 + \gamma_2}{2}\right)^{\frac{1}{\gamma_2 - 1}}} \theta(M_2) \left(\frac{A_1}{A_2}\right)$$

$$\frac{P_3}{P_0} = \frac{(P_3/P_3)^*}{(P_0/P_0)} \left(\frac{P_3}{P_0}\right) = \frac{[(\gamma_3 + 1)/2]}{P_0/P_0} \frac{\gamma_3}{\gamma_3 - 1} \left(\frac{P_3}{P_0}\right)$$

$$\frac{P_2}{P_0} = \frac{P_1}{P_0} \left[\frac{(\gamma_0 + 1) M_0^2}{2 + (\gamma_0 - 1) M_0^2} \right]^{\frac{\gamma_0}{\gamma_0 - 1}} \left[\frac{\gamma_0 + 1}{2\gamma_0 M_0^2 - (\gamma_0 - 1)} \right]^{\frac{1}{\gamma_0 - 1}}$$

$$\frac{P_2}{P_0} = \frac{(P_2/P_2)}{(P_0/P_0)} \frac{P_2}{P_0}$$

$$\frac{h_0}{h_2} = \frac{(A/A_*)_1}{(A/A_*)_2} = \frac{M_2}{M_1} \left[\frac{2 + (\gamma_0 - 1) M_1^2}{2 + (\gamma_0 - 1) M_2^2} \right]^{\frac{1}{2}} \frac{\gamma_0 + 1}{\gamma_0 - 1}$$

$$M_1^2 = \frac{2 + (\gamma_o - 1) M_o^2}{2\gamma_o M_o^2 - (\gamma_o - 1)}$$

$$q_H = c_{p3} \tau_3 - c_{p2} \tau_2$$

$$\gamma_o = \gamma_o = \gamma_2, \quad \gamma_2 \neq \gamma_3$$

The quantities T/τ , A/A_* , and p/P , which are functions of Mach number and gamma, are tabulated in many places in the literature (See, e.g., Refs. 26, 27, and 29). There are also some publications which tabulate directly the relevant functions associated with one-dimensional heat addition (See, e.g., Refs. 3, 28, and 29).

The critical total temperature $(\tau_3/\tau_o)_{CR}$ can be obtained from the expression for (τ_3/τ_o) by replacing M_2 with M_o . The critical value of (P_3/P_o) is then obtained by replacing (τ_3/τ_o) by $(\tau_3/\tau_o)_{CR}$ in the expression for (P_3/P_o) .

The functions which are of interest with regard to the application of the one-dimensional heat addition relations to the present problem are plotted in Figs. 4 through 8 for $\gamma_2 = \gamma_3 = 7/5$. For a constant gamma, and hence for a constant specific heat c_p across the heater, the heat-addition rate per unit area, q_H , is proportional to $\Delta\tau$.

In the analysis and presentation of results which follow in later sections, one has the choice of using either $(\Delta\tau/\Delta\tau_{CR})$ or the spillage, $1 - h_o^*$, as an independent variable. The spillage is selected for two reasons. First, the flow field is more easily visualized in terms of a specified spillage, particularly for the limiting cases of zero and unit spillage. Second, at a given Mach number, some of the pertinent properties of the flow ahead of the heater are a linear function of the

spillage. The correspondence between the spillage and the total temperature increase (and hence the rate of heat addition) is shown in Fig. 7. Although not shown in Fig. 7, it is of interest to note that the total temperature increase approaches infinity for spillages approaching unity. However, physically attainable cases are, in all probability, limited to spillages considerably less than unity. For the external combustion of a hydrocarbon fuel, this limitation is governed by the enthalpy of the fuel. Orders of magnitude for this case will be presented shortly. If the heat is added by means of a heat exchanger using a nuclear energy source, the upper limit of spillage will depend upon the temperature limitations imposed by the structural integrity of the heat exchanger. If the heat from a nuclear energy source could be added without consideration for structural limitations, higher spillages possibly could be achieved.

Subsequently in the analysis, in the process of developing analytical results for the complete spillage range from zero to unity the limiting case of unit spillage is utilized. In doing this, cognizance is taken of the fact that the extremely high temperatures involved when the spillage approaches unity are not compatible with the use of a constant gamma through the heater, and of the fact that the expansion downstream of the heater will be somewhat different than that for the Prandtl-Meyer expansion for an ideal gas. Nevertheless, the use of a constant gamma is believed to be an acceptable procedure for establishing the approximate flow field in the lower spillage range.

It is of interest to estimate the spillage corresponding to the external combustion of a particular fuel. This has been done for the constant pressure combustion of a stoichiometric mixture of kerosene and air in quiescent air at initial temperatures of \mathcal{T}_0 corresponding to M_0 . The

resulting total temperature increase and the corresponding spillages are shown as a function of free-stream Mach number in Fig. 9.⁴ These values serve only as a guide to orders of magnitude, since they are based on a constant pressure process, whereas the process used in this analysis involves heat addition to a constant area stream tube with an accompanying spacewise discontinuity in pressure. Note that there is no spillage possible for free-stream Mach numbers greater than $M_0 = 5.5$. Conceivably, spillage might be obtained at the higher Mach numbers through the combustion of a higher enthalpy fuel or from the use of a nuclear energy source.

The effect of a variable gamma on conditions at station 3 just downstream of the heater can be estimated for the external combustion of a hydrocarbon fuel. For a given free-stream Mach number and a given spillage, the equations at the beginning of this section yield.

$$\frac{P_{3, \gamma_3}}{P_{3, \gamma_0}} = \frac{\left(\frac{1 + \gamma_3}{2}\right)^{\frac{1}{\gamma_3 - 1}}}{\left(\frac{1 + \gamma_0}{2}\right)^{\frac{1}{\gamma_0 - 1}}}$$

$$\frac{P_{3, \gamma_3}}{P_{3, \gamma_0}} = \frac{1 + \gamma_0}{1 + \gamma_3}$$

Fig. 14 of Ref. 30 gives a minimum value of 1.25 for the gamma of the products of combustion of a stoichiometric mixture of n-octane and air. Taking $\gamma_3 = 1.25$ and $\gamma_0 = 1.40$, we obtain $P_{3, \gamma_3}/P_{3, \gamma_0} = 1.015$ and $p_{3, \gamma_3}/p_{3, \gamma_0} = 1.067$.

⁴The flame temperatures upon which these data are based are from unpublished calculations kindly supplied to the author by Waldo T. Renich of Applied Physics Laboratory of The Johns Hopkins University.

The error in P_3 , resulting from the assumption of a constant gamma, is negligible, and, although the error in p_3 is slightly large, it is tolerable in view of the generally approximate nature of the analysis.

GEOMETRY OF THE FIRST SHOCK WAVE

The assumed shock wave shape used in Moeckel's analysis (Ref. 25) is given by the expression

$$y^* = h_o^* + \beta^{-1} \sqrt{x^{*2} - x_o^{*2}}$$

The relations for the important parameters, using the continuity method of Moeckel and taking $\eta = \theta_{\rho_1}$ are found to be as follows,

$$\frac{x_o^*}{1-h_o^*} = \frac{\beta^2 \tan \varphi_{\rho_1} - C}{1 - B \cos \theta_{\rho_1}}$$

$$\frac{x_{\rho_1}^*}{1-h_o^*} = \frac{\beta^2 \tan \varphi_{\rho_1}}{1 - B \cos \theta_{\rho_1}}$$

$$y_{\rho_1}^* = 1 + \frac{(1-h_o^*) B \cos \theta_{\rho_1}}{1 - B \cos \theta_{\rho_1}}$$

$$\frac{L^*}{(1 - h_o^*)} = \frac{C + B \sin \theta_{\rho_1}}{1 - B \cos \theta_{\rho_1}}$$

$$C = \beta \left(\beta \tan \varphi_{\rho_1} - \sqrt{\beta^2 \tan^2 \varphi_{\rho_1} - 1} \right)$$

$$B = (P_o/\bar{P}) (A/A_*)_o$$

$$\frac{\bar{P}}{P_o} = \left[\frac{(\delta_o + 1) M_o^2 \sin^2 \bar{\theta}_g}{(\delta_o - 1) M_o^2 \sin^2 \bar{\theta}_g + 2} \right] \frac{\delta_o}{\delta_o - 1} \left[\frac{\delta_o + 1}{2 \delta_o M_o^2 \sin^2 \bar{\theta}_g - (\delta_o - 1)} \right] \frac{1}{\delta_o - 1}$$

$$\left(\frac{A_*}{A} \right)_o = M_o \left[\frac{\delta_o + 1}{2 + (\delta_o - 1) M_o^2} \right] \frac{1}{2} \left(\frac{\delta_o + 1}{\delta_o - 1} \right)$$

$$\tan \theta_{\rho_1} = \left[\left(\frac{(\delta_o + 1) M_o^2}{2 M_o^2 \sin^2 \varphi_{\rho_1} - 2} - 1 \right) \tan \varphi_{\rho_1} \right]^{-1}$$

$$\bar{y} = \frac{1}{2} (y_{\rho_1} - h_o) + h_o$$

$$\tan \bar{\psi} = \beta^{-1} \sqrt{4 \beta^2 \tan^2 \varphi_{\rho_1} - 3}$$

For further details the interested reader may consult Ref. 25.

The parameter $L^*/(1 - h_o^*)$, which is a function of free-stream Mach number only, is plotted on Fig. 10.

APPROXIMATE FLOW CONDITIONS AT THE INTERSECTION OF THE HEATER PLANE AND THE SECOND SHOCK WAVE

Although the second shock wave is actually curved, in the approximate analysis of this paper that portion of it near to the top of the heater is assumed to be represented "on the average" by a straight shock and to be influenced by a mean flow just upstream of the shock. This mean flow is characterized by a mean total pressure \bar{P} , and a mean Mach number \bar{M} , and a mean flow direction $\bar{\theta}$. The shock wave strength and inclination are dependent upon the mean upstream flow, and the boundary conditions, to be described subsequently, at the intersection of the heater and the interface.

In attempting to describe grossly the dynamics of the flow in the region of point G of Fig. 1, it seems reasonable to consider an amount of spilled mass-flow equal in magnitude to the mass flow through the heater. Such a mass flow is illustrated by the flow between the streamlines $\overline{DA\delta_2}$ and \overline{JEF} shown in Fig. 1. The mean streamline \overline{jefg} with free-stream ordinate $\bar{y} = 3h_o/2$, is representative of this mass flow and is therefore used in the determination of \bar{P} , \bar{M} , and $\bar{\theta}$.

Downstream of the first shock wave the flow is isentropic along the streamline \overline{efg} , therefore the mean total pressure \bar{P} is the total pressure aft of the first shock at the ordinate $y_e = \bar{y} = 3h_o/2$ on the wave. The shock wave angle φ_e corresponding to y_e , as determined from the geometric

relations given in the previous section, is

$$\psi_e = \tan^{-1} \left[\frac{1}{\beta} \sqrt{1 + \frac{4X_o^{*2}}{\beta^2 h_o^{*2}}} \right]$$

The relation for x_o^* is given in the previous section.

Now, let us denote by $(1 - h_o^*)_{\Delta_1}$ the spillage corresponding to the passage of the streamline \overline{JEF} through the point Δ_1 shown in Fig. 1. The streamline \overline{JEF} will pass above y_{Δ_1} when the spillage is less than $(1 - h_o^*)_{\Delta_1}$, and below y_{Δ_1} , as shown in the figure, when the spillage is greater than $(1 - h_o^*)_{\Delta_1}$. For spillage greater than $(1 - h_o^*)_{\Delta_1}$, we shall assume that the stream tube $\overline{JEF} - \overline{DA\Delta_2}$ is approximated by a Prandtl-Meyer expansion of the streamline \overline{fg} through the angle $\Omega - \bar{\theta}$. Knowing $\bar{\theta}$, the mean Mach \bar{M} is obtainable from the Prandtl-Meyer relations. The method for determining $\bar{\theta}$ will be described subsequently.

For spillages less than $(1 - h_o^*)_{\Delta_1}$, this simple method for obtaining \bar{M} is no longer applicable, since the upper streamline of the streamtube $\overline{DA\Delta_2} - \overline{JEF}$ crosses the first shock above the sonic point Δ_1 , and hence the streamtube flow "on the average" cannot be considered as having executed a Prandtl-Meyer expansion. The method for determining \bar{P} is still applicable, however, regardless of the amount of spillage. As a consequence of its restriction to a specific spillage range, the foregoing method for determining \bar{M} is called the "restricted method" to avoid confusion with the "final method" which is developed later. The final method is valid for the complete spillage range, i.e., from zero to unity.

As a prerequisite to the derivation of the final method it is first necessary to consider some consequences of the restricted method. In order to do this the boundary conditions at the point G in Fig. 1 are required.

With reference to Fig. 1, the boundary conditions for a specified super-critical heat-addition rate require an oblique second shock wave angle for which $p_4 = p_5$ and $\theta_4 = \theta_5$. Noting that $(p_4/P_0) = (p/P) \gamma_4 (P_3/P_0)$, and $(p_5/P_0) = (p_5/\bar{p}) (\bar{p}/P_0)$, these boundary conditions yield

$$\frac{P_3/P_0}{(\bar{p}/\bar{P}) (\bar{P}/P_0)} = \frac{p_5/\bar{P}}{(p/P) \gamma_4}$$

$$\theta_4 = \theta_5$$

For a specified free stream Mach number and heat-addition rate (or spillage), and a known value of $\bar{\theta}$, the left hand side of the first equation is known. Solution for the shock wave angle $\bar{\phi}$ which simultaneously satisfies both of the above equations must be obtained by trial and error. Since the mechanics of this process can be performed many different ways, no specific procedure is described here.

We now investigate, by means of the restricted method, the consequences of assigning upper and lower limiting values to $\bar{\theta}$. The upper limit, $\bar{\theta}_u$, is that value of $\bar{\theta}$ for which the second shock wave becomes a Mach wave. In this case $\bar{\theta} = \bar{\theta}_u = \theta_4$. The lower limit, $\bar{\theta}_l$, is that value of $\bar{\theta}$ for which sonic velocity exists behind the second shock wave.

Values of θ_4 , corresponding to the upper and lower values of $\bar{\theta}$, are shown by the solid lines in Fig. 11 for free-stream Mach numbers of 2, 3, 5, and 7, and for spillage values ranging from $(1 - h_o^*)_{\rho_1}$ to unity. Also shown, are the values of θ_4 for zero spillage. For a given free-stream Mach number, $\bar{\theta}_l$ varies slightly with spillage. A representative value of $\bar{\theta}_l$ along with its possible deviation in the restricted spillage range is given for each lower limit curve.

It is observed in Fig. 11 that the value of θ_4 for a given free-stream Mach number is relatively insensitive to $\bar{\theta}$. Therefore, the flow in the region enclosed by the heater, the wall, and the last Prandtl-Meyer characteristic (i.e., the region within Gx_3x_m in Fig. 1) is also relatively unaffected by $\bar{\theta}$. The flow downstream of the last Prandtl-Meyer characteristic, however, is affected by $\bar{\theta}$ via the mean inclination, $\bar{\Phi}$, of the second shock wave. The influence of $\bar{\theta}$ on the mean inclination of the second shock wave is illustrated in Fig. 12 for the upper and lower limiting values of $\bar{\theta}$.

It will be shown in a subsequent section that the major portion of the aft normal force is obtained from the region between the heater and the last Prandtl-Meyer characteristic. Consequently, if the primary interest is in plate forces, and not flow-field details, the value of $\bar{\theta}$ which is used is not especially critical. With this in mind, the flow angle $\bar{\theta}$ will be taken as zero, on the basis of the assumption that the mean over-the-top stream behaves as if it were flowing parallel to the flat top of a heater of finite thickness.

Values of θ_4 calculated by the restricted method using a zero value for $\bar{\theta}$ are shown by the appropriately labeled solid lines in Fig. 11.

Since the values of θ_4 for zero spillage are known, it seems reasonable to obtain values of θ_4 in the region for

which a theory has not yet been advanced, i.e., for $0 \leq (1 - h_o^*) \leq (1 - h_o^*)_{\Delta_1}$, by simply assuming the interpolated curves shown by the dashed lines in Fig. 11. It is seen that the resulting curves, for the complete spillage range from zero to unity, yield almost constant values of θ_4 for a fixed free-stream Mach number. In view of the generally approximate nature of the analysis it is appropriate, for a fixed free-stream Mach number, to consider θ_4 (and hence v_4) as constant with respect to spillage. This constant value is taken as that corresponding to zero spillage rather than an average over the complete spillage range, since the zero spillage value may be determined exactly. Hence, in the "final method" θ_4 is known "a priori" and is a function only of free-stream Mach number.

The effect of an error in θ_4 on the aft normal force is analyzed in a later section dealing with the normal forces.

The "final method" for approximately analyzing the flow over the top of the heater is summarized as follows. Referring to Fig. 1, the flow is considered to be represented by the mean streamline \overline{jefg} previously described. The mean total pressure \overline{P} along \overline{efg} , downstream of the second shock wave, is that value of the total pressure aft of the first shock wave at the ordinate $y_e = 3h_o/2$ on the wave. The mean streamline \overline{fg} , in passing over the top of the heater, is considered to expand from a Mach number of unity at the point f through a Prandtl-Meyer expansion to a final flow direction $\overline{\theta} = 0$. In the restricted method the Prandtl-Meyer angle for the mean flow was considered to be known and θ_4 was to be determined. In the final method θ_4 is known for a specified free-stream Mach number. The Prandtl-Meyer angle for the mean flow, and the corresponding \overline{M} , is determined by the shock-interface conditions which are governed by the known value of θ_4 . In

this approach, the inclination of the sonic line at the point f is considered to be slightly different than η .

The mean Mach number \bar{M} and the mean second shock-wave angle $\bar{\Phi}$, calculated on the basis of the final method are shown as functions of spillage and free-stream Mach number in Fig. 13. These curves are not actually needed for the determination of the aft normal force, but are presented as a matter of interest.

THE DOWNSTREAM PRESSURE DISTRIBUTION

As mentioned in the section describing the mathematical model, the approximate downstream pressure distribution from x_3^* to x_m^* is calculated on the basis of a simply reflected Prandtl-Meyer expansion. For downstream distances greater than x_m^* the pressure distribution is assumed to be given approximately by a two-parameter descending exponential variation with x^* .

In this section, the necessary relations for the use of these approximations are presented along with their limitations and a partial verification of their appropriateness.

With reference to Fig. 1, consider any general right-running Prandtl-Meyer characteristic centered at the point G. The geometry shown in the figure for the last Prandtl-Meyer characteristic, denoted by the subscript "m", will serve for a general Prandtl-Meyer characteristic if the subscript "m" is replaced by the subscript "R". The characteristic constant (Refs. 31 and 32) for a general right-running Prandtl-Meyer characteristic is $(\nu_R + \theta_R)$ or $(2\nu_R)$, since $M_3 = 1.0$. This characteristic makes the angle $(\theta_R - \mu_R)$, or $(\nu_R - \mu_R)$, with the plate (See Fig. 1). If we denote quantities at the intersection of a characteristic and the wall by symbols without a subscript, we obtain the relation

$(\gamma + \theta) = 2 \gamma_R$. Since $\theta = 0$, this becomes

$$\gamma = 2 \gamma_R$$

The x^* -coordinate of the intersection is given by

$$x^* - x_3^* = \cot (\mu_R - \theta_R) = \cot (\mu_R - \gamma_R)$$

The pressure ratio p/p_3 at x^* is then obtained from

$$\frac{p}{p_3} = \frac{(p/P)_{\gamma = 2 \gamma_R}}{(p/P)_*}$$

where

$$(p/P)_* = \left[(\delta + 1)/2 \right]^{-\frac{\delta}{\delta - 1}} = 0.52283 \quad (\delta = 1.4)$$

The pressure ratio p/P as a function of γ is available in numerous tables (See, e.g., Ref. 26).

It is convenient to record some properties of a simply-reflected Prandtl-Meyer expansion for which the last characteristic intersects the x -axis at infinity. The downstream distribution of wall pressure, denoted by \tilde{p} for this case, is plotted in Fig. 14. The value of \tilde{p} at infinity, \tilde{p}_∞ , is obtained by noting that $\gamma_R = \mu_R$ at infinity. From the Prandtl-Meyer relation (See Eq. 171, Ref. 26) we obtain

$$\gamma_R = \mu_R = \cot^{-1} \left[\frac{\sqrt{\delta + 1}}{\sqrt{\delta - 1}} \tan \left(90^\circ \sqrt{\frac{\delta - 1}{\delta + 1}} \right) \right]$$

For $\delta = 1.4$, this yields $\gamma_R = \mu_R = 28.63^\circ$, and hence $\gamma = 57.26^\circ$. The corresponding value of \tilde{p}/p_3 is $(\tilde{p}/p_3)_\infty = 0.0278$.

The pressure distribution downstream of x_m^* is assumed to be given approximately by the relation

$$\frac{p_{11} - p_0}{p_3} = \left(\frac{\tilde{p}_{11_m} - p_0}{p_3} \right) \exp \left[-b(x^* - x_m^*) \right] \quad (b \leq 0) \quad (1)$$

where the parameter "b" is determined so that the first derivative of the pressure distribution matches that for the simply reflected Prandtl-Meyer expansion at the point x_m^* . Hence we obtain

$$b = - \frac{\left[\frac{d(\tilde{p}_{11}/p_3)}{d(x^* - x_3^*)} \right]_{x^* = x_m^*}}{\left(\frac{\tilde{p}_{11_m} - p_0}{p_3} \right)} \quad (2)$$

The analytical relation for the derivative in Eq. (2) is given in the Appendix. The derivative itself is plotted on Fig. 15.

The foregoing approximation is limited to cases where $\tilde{p}_{11_m} \geq p_0$, since for $\tilde{p}_{11_m} < p_0$, it is no longer possible to approximate the pressure distribution downstream of x_m^* by a

simple monotonic variation such as given by Eq. (1). For $M_o \geq 2.58$, \tilde{p}_{11_m} is always greater than p_o , regardless of the amount of spillage. For free-stream Mach numbers less than 2.58, there exists for each Mach number, a limiting spillage value above which \tilde{p}_{11_m} is less than p_o . At $M_o = 2.0$, for example, this limiting spillage value is 1.35. The limiting spillage value becomes zero at $M_o = 1.50$. Hence, the approximation cannot be applied in any case for a free-stream Mach number less than 1.50.

In order to partially verify the appropriateness of the approximate solution, method of characteristics calculations have been made for the downstream flow for critical heat addition at free-stream Mach numbers of two and six. The characteristics calculations were performed assuming irrotational flow and using a lattice-point method with a numerical-graphical procedure (Refs. 31 and 32). The previously described boundary conditions at the interface were satisfied by a trial and error process. The resulting characteristic nets are shown in Figs. 16 and 17. The fact that the shock curvature is very small in both cases substantiates the assumption of irrotational flow used in the calculations. Although the wall-pressure distribution is of principal concern here, the characteristic constants for the flow are given in Table I as a matter of interest.

Comparisons of the downstream wall-pressure distributions as calculated by the approximate method and the characteristics method are shown in Fig. 18. It is seen in these figures that the two methods are in excellent agreement for the $M_o = 2.0$ case, and in fair agreement for the $M_o = 6.0$ case. Note that the agreement is excellent at both Mach numbers in the region where the simply reflected Prandtl-Meyer expansion is used. Considering the characteristics

solution to be an exact one, the ratio of the approximate normal force to the exact normal force at several x^* -stations is as follows. For a free-stream Mach number of two, the ratio is 0.98, 0.94, and 0.94 respectively at $(x^* - x_3^*) = 2, 4, \text{ and } 6$, while for a free-stream Mach number of six it is 0.92, 0.85, and 0.79 respectively at $(x^* - x_3^*) = 6, 8, \text{ and } 10$.

A question arises with regard to the downstream existence or non-existence of imbedded oblique-shock or Mach-shock reflections such as are known to occur in jets exhausting into supersonic streams (See, e.g., Refs. 33 and 34). If such imbedded shocks actually do occur in the present case, the monotonic pressure distribution assumed herein does not properly represent the pressure discontinuities of shock waves. Because of the paucity of information dealing with both sonic and supersonic jets exhausting into supersonic streams (Ref. 33), it is not possible to use such information to make predictions regarding the appearance or non-appearance of imbedded shocks in the present problem. It is conjectured by the writer that such shocks are more likely to occur when $\tilde{p}_{11_m} < p_o$. This is, of course, outside the range of applicability of the present approximation. If imbedded shocks do actually occur within the range of applicability of the approximate method, there is a reasonable possibility that the pressure jumps associated with these shocks are small compared with the pressure drop in the region up to the last Prandtl-Meyer characteristic (See Ref. 34 for an example of this situation). Briefly, since the greater part of the downstream force exists in the region up to the Prandtl-Meyer expansion⁵, it is reasoned that the force downstream

⁵This may be observed in Fig. 19 which is discussed in a later section.

of x_m^* may be calculated on the basis of a pressure distribution which represents the actual distribution only in a rather gross manner.

It is of interest to note that the Mach 2.0 case of Fig. 16, with $P_3/p_0 = 5.22$, corresponds rather closely to the conditions of some experimental results reported by Rousso and Baughman (Ref. 35) for a sonic jet exhausting into a Mach 1.91 supersonic stream. The major difference is that the Rousso-Baughman tests are for an axially-symmetric jet, whereas the present calculations are for two-dimensional flow. Ref. 35 presents schlieren photographs of the jet exhaust for values of P_3/p_0 equal to 4.6 and 10.0. For both of these cases (bracketing $P_3/p_0 = 5.22$ for Fig. 16) shock waves are observed in the jet within a distance of four jet radii downstream. The diagram of Fig. 16 reveals no shocks within this region. Although these situations are not exactly comparable, the fact that there is not even a qualitative similarity between the flows is somewhat puzzling.

THE NORMAL FORCES

The forward normal force coefficient per unit width, Y_{10}^* , acting on the surface $\overline{x_0 x_2}$ is

$$Y_{10}^* = -q_0^{-1} \int_{x_0^*}^{x_2^*} (p_{10} - p_0) dx^* \quad (3)$$

Applying the momentum theorem to the fluid enclosed within the control region $x_0^* x_2^* \rho_2 \rho_1 x_0^*$, and assuming that \bar{a} is normal to $\overline{\rho_1 \rho_2}$, we obtain

$$Y_{10}^* = - q_o^{-1} (\bar{p} + \bar{\rho} \bar{a}^2 - p_o) (x_2^* - x_{\rho_1}^*)$$

or

$$Y_{10}^* = (2/\delta M_o^2) [(\delta + 1) (\bar{p}/p_o - 1)] (x_2^* - x_{\rho_1}^*)$$

Writing $(x_2^* - x_{\rho_1}^*)$ in terms of the flow variables and taking $\eta = \theta_{\rho_1}$, we obtain

$$\frac{Y_{10}^*}{1 - h_o^*} = - \frac{2}{\delta M_o^2} [(\delta + 1) (\bar{p}/p_o) - 1] \left(\frac{B \sin \theta_{\rho_1}}{1 - B \cos \theta_{\rho_1}} \right) \quad (4)$$

where $B = (P_o/\bar{P})(A/A_o)_o$. The quantity $Y_{10}^*/(1 - h_o^*)$, which is a function only of M_o , is plotted on Fig. 10.

The forward moment coefficient per unit width, M_{10}^* , for the surface $\overline{x_o x_2}$, with moments taken about the point x_o , is

$$M_{10}^* = \int_{x_o^*}^{x_2^*} (x^* - x_2^*) C_{p10} dx^* \quad (5)$$

It is assumed that the pressure distribution along $\overline{x_o x_2}$ is given approximately by

$$C_{p10} = C_{p1} + a_1 (x^* - x_o^*) + a_2 (x^* - x_o^*)^2 \quad (6)$$

The coefficients α_1 and α_2 are determined by the condition that $C_{p10} = C_{p2}$ when $(x^* - x_0^*) = L^*$ and by the condition that Y_{10}^* is obtained when the Eq. (6) is substituted in Eq. (3). The condition that $C_{p10} = C_{p1}$ at $(x^* - x_0^*) = 0$ is automatically satisfied by Eq. (6). Evaluation of the coefficients α_1 and α_2 and substitution of the resulting expression for C_{p10} in the moment relation yields

$$M_{10}^* = (L^{*2}/2) \left[(Y_{10}^*/L^*) + \frac{1}{6} (C_{p2} - C_{p1}) \right] \quad (7)$$

The aft normal force coefficient per unit width, Y_{11}^* , acting on the downstream wall in the region from x_3^* to x^* is

$$Y_{11}^* = -q_0^{-1} \int_{x_3^*}^{x^*} (p_{11} - p_0) dx^* \quad (8)$$

The particular expression which must be used for Y_{11}^* depends upon whether x^* is greater than or less than x_m^* .

The aft normal force coefficient for $x^* \leq x_m^*$ is

$$Y_{11}^* = - (p_3/q_0) \tilde{I}_0 + (p_0/q_0) (x^* - x_3^*)$$

where

$$\tilde{I}_0 = \int_0^{x^* - x_3^*} (\tilde{p}_{11}/p_3) d(x^* - x_3^*) \quad (9)$$

The integral \tilde{I}_O has been evaluated numerically. Its variation with $(x^* - x_3)$ is presented in Fig. 15.

The aft normal force coefficient for $x^* \geq x_m^*$ is

$$Y_{11}^* = Y_{11m}^* - (p_3/q_0) J_O \quad (10)$$

where Y_{11m}^* is the value of Y_{11}^* given by Eq. (9) when $x^* = x_m^*$, and

$$J_O \equiv \int_{x_m^*}^{x^*} \left[(p_{11} - p_0)/p_3 \right] dx^* \quad (11)$$

Substituting Eq. (1) in Eq. (11) and evaluating the integral yields

$$J_O = b^{-1} (\tilde{p}_m/p_3 - p_0/p_3) \left\{ 1 - \text{EXP}[-b(x^* - x_m^*)] \right\} \quad (12)$$

where "b" is given by Eq. (2).

The aft moment coefficient per unit width, \mathcal{M}_{11}^* , acting on the downstream wall in the region from x_3^* to x^* is

$$\mathcal{M}_{11}^* = (1/q_0) \int_{x_3^*}^{x^*} (x^* - x_3^*) (p_{11} - p_0) dx^* \quad (13)$$

In a manner analogous to that for the normal force, the particular expression which must be used for \mathcal{M}_{11}^* depends upon

whether x^* is greater than or less than x_m^* .

The aft moment coefficient for $x^* \leq x_m^*$ is

$$m_{11}^* = - (p_3/q_0) \tilde{I}_1 - \frac{1}{2} (p_0/q_0) (x^* - x_3^*)^2 \quad (14)$$

where

$$\tilde{I}_1 \equiv \int_0^{x^* - x_3^*} (x^* - x_3^*) (\tilde{p}_{11}/p_3) d(x^* - x_3^*)$$

The integral \tilde{I}_1 has been evaluated numerically. Its variation with $(x^* - x_3^*)$ is presented in Fig. 15.

The aft moment coefficient for $x^* \geq x_m^*$ is

$$m_{11}^* = m_{11_m}^* + (p_3/q_0) J_1 \quad (15)$$

where $m_{11_m}^*$ is the value of m_{11}^* given by Eq. (14) when $x^* = x_m^*$, and

$$J_1 \equiv \int_{x_m^*}^{x^*} (x^* - x_3^*) \left[(p_{11} - p_0)/p_3 \right] d(x^* - x_3^*) \quad (16)$$

Substituting Eq. (1) in Eq. (16) and evaluating the resulting integral yields

$$J_1 = - \left(\frac{x^* - x_m^*}{b} \right) \left(\frac{p_m - p_o}{p_3} \right) + \left[(x^* - x_3^*) + \frac{1}{b} \right] J_o \quad (17)$$

The center of pressure is given by

$$x_{cp}^* - x_3^* = - \frac{M_{10}^* + M_{11}^*}{\bar{I}_{10}^* + Y_{11}^*} \quad (18)$$

The cumulative aft normal force coefficient as a function of downstream position for zero spillage is plotted in Fig. 19 for free-stream Mach numbers of 2, 3, 5, and 7 respectively. Also shown on this figure is the x^* -coordinate, x_m^* of the last Prandtl-Meyer expansion. It can be seen, as was previously stated, that the major portion of the normal force is achieved in the region of the simply reflected Prandtl-Meyer expansion.

The curves for other spillages are not greatly different from those shown in Fig. 19 due to the fact that γ_4 is independent of spillage and to the fact that the variation of C_{p_3} with spillage is moderate (See Fig. 8).

Also shown in Fig. 19 is the normal-force coefficient for an infinitely long plate. Since it is obviously impractical to expand to infinity it is necessary to select some other suitable reference force and length at which to terminate the expansion. From examination of the figure it is apparent, that in general, there is little to be gained by expanding beyond the station where approximately nine-tenths of the infinite-plate aft normal force is reached. Consequently, for all spillages at a given free-stream Mach number, the reference length (i.e., the length at which it is practical to terminate the plate) will be taken as x_t^* ,

where x_t^* is the station at which the normal force is nine-tenths the infinite-plate aft normal-force at zero spillage. Values of $x_t^* - x_3^*$ are indicated on Fig. 19. The aft normal-force coefficient corresponding to x_t^* is denoted by $Y_{11_t}^*$, while the corresponding total normal-force coefficient is denoted by Y_t^* .

The total normal-force coefficient Y_t^* , and the forward normal-force coefficient Y_{10}^* as functions of free-stream Mach number are shown in Fig. 20. The limitation on Y_t^* for $M_0 = 2.0$ is due to the fact the analysis fails to provide a solution when $\tilde{p}_m \leq p_0$. It may be observed, that $Y_{11_t}^*$ is almost independent of spillage, since the curves of Y_t^* and Y_{10}^* are almost parallel for a given free-stream Mach number. It is also of interest to note that with increasing spillage the forward normal force becomes an increasingly larger fraction of the total force.

In Fig. 21 there is shown the average normal force coefficient per unit length for a flat plate terminated at x_t^* as a function of spillage and free-stream Mach number. It is seen here that the average force per unit length increases with spillage. A cross-plot of Fig. 21 at zero spillage reveals a maximum average normal force per unit length at $M_0 = 2.5$. This maximum either disappears or moves to a lower Mach number very rapidly with increased spillage. This point has not been explored further because the present method is inapplicable below $M_0 = 1.5$, and because the spillage range for which it is valid for Mach numbers less than 2.68 diminishes very rapidly with decreasing Mach number. It is also probable that practical applications will tend towards the higher Mach numbers.

The center of pressure of a flat plate terminated at x_t^* as a function of spillage and free-stream Mach number as shown in Fig. 22.

It will be recalled that the present analysis is based on the assumption that θ_4 is independent of the spillage for a given free-stream Mach number, whereas Fig. 11 indicates there exists a range of possible values for θ_4 for a given Mach number. With reference to Fig. 19, it may be observed that x_t^* is less than x_m^* for the curves corresponding to Mach numbers of 2, 3, and 5. Therefore, since θ_4 does not influence Y_{11}^* (except indirectly through the establishment of x_t^*), the precise determination of θ_4 is not important. This observation is also true for the complete spillage range. For $M_o = 7.0$, Y_{11}^* is influenced by θ_4 , since x_t^* is greater than x_m^* . The selection of x_t^* , however, is somewhat arbitrary. If a slightly different criterion for its selection had been used, it is possible that x_t^* could have been larger than x_m^* for all Mach numbers within the range treated.

Regardless of the specific criterion used for the selection of x_t^* there is little to be gained by selecting x_t^* much larger than x_m^* , since as we progress downstream most of the aft infinite-plate normal force is achieved when x_m^* is reached. For example, for Fig. 19, the force ratio, $Y_{11_m}^*/Y_{11}^*$, has values of 1.00, 0.98, 0.92, and 0.88 respectively for Mach numbers of 2, 3, 5, and 7. The corresponding values for other spillages are within about 2 per cent of these. Since Y_{11}^* is a reasonably good measure of the downstream force which we desire, an estimate will be made of the effect of an error in θ_4 on the value of $Y_{11_m}^*$. From Eq. (9), we obtain

$$\frac{d Y_{11_m}^* / d \theta_4}{Y_{11_m}^*} = \left[\frac{\frac{d \tilde{I}_o}{d(x_m^* - x_o^*)} - \frac{p_o}{p_3}}{\tilde{I}_o - \frac{p_o}{p_3}} \right] \frac{d(x_m^* - x_3^*)}{(x_m^* - x_3^*)}$$

where

$$\frac{d \tilde{I}_o}{d (x_m^* - x_o^*)} = \left(\frac{\tilde{p}_{11}}{p_3} \right)_{x_m^*} \left[\frac{d (\tilde{p}_{11}/p_3)}{d (x_m^* - x_3^*)} \right]_{x_m^*}$$

The derivative $d(x_m^* - x_3^*)/d\theta_4$ is available in the Appendix. The other properties of a simply reflected Prandtl-Meyer expansion are plotted on Figs. 14 and 15. The pressure ratio p_o/p_3 may be obtained from Fig. 8.

The consequence of applying the above relations are displayed in the table below.

M_o	p_o/p_3	θ_4	$\frac{d Y_{11_m}/d\theta_4}{Y_{11_m}}$	$\Delta\theta_4$	$\frac{\Delta Y_{11_m}}{Y_{11_m}}$
		DEG	1/DEG	DEG	
2	0.3948 (±0.0312)	8-10	-0.15	-0.5 +0.2	+0.08 -0.03
3	0.1877 (±0.0113)	12-16	-0.06	-1.3	+0.09
5	0.0700 (±0.0034)	16-18	-0.03	-1.7	+0.06
7	0.0361 (±0.0017)	18-22	-0.02	-1.7 -0.2	+0.04 0

Since the purpose of this table is to indicate orders of magnitude, a representative value of p_o/p_3 for the complete spillage range at each Mach number is used in lieu of showing the variation with spillage. The range of possible

deviations is given in parenthesis under each of the tabulated representative values. The value of $(dY_{11_m}/d\theta_4)Y_{11_m}^{-1}$ listed is the largest value for the given θ_4 range. The smallest value for each Mach number is, on the average, 0.01 less in absolute magnitude than the tabulated value. The possible error, $\Delta\theta_4$, is the maximum and/or minimum deviation of the zero spillage value of θ_4 from the curves shown in Fig. 11. The error in $Y_{11_m}^*$ corresponding to $\Delta\theta_4$ is recorded in the last column in the table. It is seen here that the error decreases with increasing Mach number. Although the error in $Y_{11_m}^*$ at the lower Mach numbers is slightly larger than one might desire, it is tolerable in view of the approximate nature of the analysis.

A final point of interest is the possible influence of the intersection of the first and second shock waves on the downstream pressure distribution, and hence on the aft normal force. For a straight second shock, with inclination $\bar{\Phi}$, it is easy to calculate the intersection of the two shocks. The results of such a calculation are shown in Fig. 23. The coordinates of the point of intersection of these shocks are given by the solid-line curves on Fig. 23. Note that the trace of the intersection of the shock-waves is almost independent of Mach number for the Mach number range shown. The flow inclination, θ_I , downstream of the first shock, and neglecting interaction with the second shock, is also shown in Fig. 23, along with lines of constant spillage corresponding to θ_I . It can be seen from these curves that when the intersection is close to the heater θ_I is large, the intersection is relatively far away, so that the strong interaction in all probability will be transmitted relatively far downstream. This favorable behavior becomes less pronounced for increasing free-stream Mach numbers.

CONCLUDING REMARKS

On the basis of a simplified model and an approximate theoretical analysis thereof, calculations have been made, and charts presented, for the pertinent flow-field parameters and the normal forces and moments for the super-critical addition of heat to the external flow about a supersonic airborne vehicle. With due consideration for their limitations, these charts should serve to obtain approximate estimates of the performance of vehicles utilizing this mode of propulsion and/or lift production.

Application of the method to the estimation of the performance of a specific vehicle configuration is considered to be beyond the scope of this paper.

For the model analyzed, the most salient characteristic is that the normal-force increase due to increased super-critical heat addition at a constant Mach number is obtained almost entirely from the region forward of the heater; the aft normal force is almost constant with increasing heat addition. The percentage contribution of the forward normal force to the total normal force varies from zero at zero spillage to about sixty to eighty per cent, depending upon the Mach number, at unit spillage.

APPENDIX

DERIVATIVE OF THE WALL-PRESSURE DISTRIBUTION FOR A SIMPLY REFLECTED PRANDTL-MEYER EXPANSION

The detailed derivation of the derivative will not be given here since it is relatively easy to reproduce. Consider a Prandtl-Meyer expansion from $M_3 = 1.0$ with the orientation shown in Fig. 1, except for a coordinate shift so that $x_3^* = 0$. Denote quantities associated with an unreflected right-running Prandtl-Meyer characteristic prior to its intersection with the wall by the subscript "R". Quantities at the wall are without a subscript. The relations used are the Bernoulli equation, the Prandtl-Meyer relation, the Mach angle relation, the geometry of the intersection, and the reflected characteristic relation, $\psi = 2\psi_R$. Using these we obtain the following result,

$$\frac{d(p/p_3)}{dx^*} = \left[\frac{d(p/p_3)}{dM} \right] \frac{d\theta_R/dx^*}{d\theta_R/dM}$$

where

$$\frac{d(p/p_3)}{dM} = \frac{-2\gamma M}{[2 + (\gamma - 1)M^2]} \left(\frac{p}{p_3} \right)$$

$$\frac{d\theta_R}{dM_R} = \frac{1}{M_R \beta_R} \left[\frac{M_R^2}{1 + \left(\frac{\gamma - 1}{\gamma + 1} \right) \beta_R^2} - 1 \right]$$

$$\frac{d\theta_R}{dx^*} = (1 + x^{*2})^{-1} \left[1 + \frac{1}{M_R \beta_R (d\theta_R/dM_R)} \right]$$

REFERENCES

1. Chambre, Paul, and Lin, C. C.: On the Steady Flow of a Gas Through a Tube with Heat Exchange or Chemical Reaction. *Journal of Aeronautical Sciences*, Vol. 13, No. 10, October 1946, pp. 537-542. For discussions, see *JAS* 1947, January pp. 24 and 63, May pp. 293-294, October p. 600.
2. Hicks, Bruce L., Montgomery, Donald J., and Wasserman, Robert H.: The One-Dimensional Theory of Steady Compressible Fluid Flow in Ducts with Friction and Heat Addition. *NACA TN 1336*, July 1947. Also see, *Jour. Appl. Physics*, Vol. 18, No. 10, Oct. 1947, pp. 891-903.
3. Shapiro, Ascher H., and Hawthorne, W. R.: The Mechanics and Thermodynamics of Steady One-Dimensional Gas Flow, *Jour. of Appl. Mech.*, Vol. 14, No. 4, Dec. 1947, pp. A317-A336. Also see, *Handbook of Supersonic Aerodynamics NAVORD REPT 1488*, Vol. I, April 1950, pp. 4.1-4.58, and Shapiro, Ascher H.: *The Dynamics and Thermodynamics of Compressible Fluid Flow*, Vol. I, The Ronald Press Co.; New York, 1953.
4. Foa, J. V., and Rudinger, G.: On the Addition of Heat to a Gas Flowing in a Pipe at Subsonic Speed. *Jour. of Aero. Sci.*, Vol. 16, No. 2, Feb. 1949, pp. 84-94 and p. 119. For discussions, see *JAS*, Sept. 1949, p. 566, May 1949, p. 317, June 1949, p. 379, Nov. 1949, p. 699.
5. Foa, Joseph V., and Rudinger, George: On the Addition of Heat to a Gas Flowing in a Pipe at Supersonic Speed. *Cornell Aero. Lab. Rept. No. HF-534-A-2*, Feb. 19, 1949.
6. Hicks, B. L.: Diabatic Flow of a Compressible Fluid. *Quart. of App. Math.*, Vol. VI, No. 3, Oct. 1948, pp. 221-237.
7. Tsien, H. S., and Beilock, M.: Heat Source in a Uniform Flow. *Jour. of Aero. Sci.*, Vol. 16, No. 12, Dec. 1949. p. 756.
8. Hicks, B. L., Hebrank, W. H., and Kravitz, S.: Comments on Heat Source in a Uniform Flow. *Jour. of Aero. Sci.*, Vol. 17, No. 9, Sept. 1950, pp. 595-596.
9. Hicks, B. L., Hebrank, W. H., and Kravitz, S.: On the Characterization of Fields of Diabatic Flow. *BRL Rept. No. 720*, Aberdeen Proving Ground, Maryland. July 1950.

10. Hicks, Bruce L.: An Extension of the Theory of Diabatic Flow. *Phys. Rev.*, Vol. 77, No. 2, Jan. 1950, p. 286. Also see, BRL Tech. Note No. 191, Aberdeen Proving Ground, April 1950.
11. Hicks, Bruce L.: On the Characterization of Fields of Diabatic Flow. *Quart. Appl. Math.*, Vol. 6, No. 4, Jan. 1949, pp. 405-416. Also see BRL Rept. No. 633, Aberdeen Proving Ground, Maryland, Oct. 1948.
12. Pinkel, I. Irving, and Serafini, John S.: Graphical Method for Obtaining Flow Field in a Two-Dimensional Supersonic Stream to which Heat is Added. NACA TN 2206, Nov. 1950.
13. Tsien, H. S.: Influence of Flame Front on the Flow Field. *Jour. of Appl. Mech.*, Vol. 18, No. 2, June 1951, pp. 188-194.
14. Blackshear, Perry L., Jr.: Driving Standing Waves by Heat Addition. NACA TN 2772, 1952.
15. Chu, Boa-Teh: Mechanism of Generation of Pressure Waves at Flame Fronts. NACA TN 3683, 1956.
16. Tchen, Chan-Mou: Heat Delivery in a Compressible Flow and Applications to Hot-Wire Anemometry, NACA TN 2436, August 1951.
17. Pinkel, I. I., Serafini, J. S., and Gregg, J. L.: Pressure Distribution and Aerodynamics Coefficients Associated with Heat Addition to Supersonic Air Stream Adjacent to Two-Dimensional Supersonic Wing. NACA RM E51K26. February 1952.
18. Gazley, Carl, Jr.: Linearized Solution for Heat Addition at the Surface of a Supersonic Airfoil. The Rand Corp. EM-1892, ASTIA Doc. No. AD133025, November 1956.
19. Mager, Artur: Supersonic Airfoil Performance with Small Heat Addition. *Journal of Aero/Space Sciences*, Vol. 26, No. 2, Feb. 1959, pp. 99-107.
20. Willmarth, W. W.: The Production of Aerodynamic Forces by Heat Addition on External Surfaces of Aircraft. The Rand Corp. RM-2078, Dec. 1957.
21. Fletcher, Edward A., Dorsch, Robert G., and Gerstein, Melvin: Combustion of Aluminum Borohydride in a Supersonic Wing Tunnel. NACA RM E55D07a, June 1955.

22. Dorsch, Robert G., Serafini, John S., and Fletcher, Edward A.: A Preliminary Investigation of Static Pressure Changes Associated with Combustion of Aluminum Borohydride in a Supersonic Wind Tunnel. NACA RM E55F07, Aug. 1955.
23. Dorsch, Robert G., Serafini, John S., and Fletcher, Edward A.: Exploratory Investigation of Aerodynamic Effects of External Combustion of Aluminum Borohydride in Air-steam Adjacent to Flat Plate in Mach 2.46 Tunnel. NACA RM E57E16, July 1957.
24. Serafini, John S., Dorsch, Robert G., and Fletcher, Edward A.: Exploratory Investigation of Static- and Base-Pressure Increases Resulting from Combustion of Aluminum Borohydride Adjacent to Body of Revolution in Supersonic Wind Tunnel. NACA RM E57E15, Oct. 1957.
25. Moeckel, W. E.: Approximate Method for Predicting Form and Location of Detached Shock Waves Ahead of Plane or Axially Symmetric Bodies. NACA TN 1921, July 1949.
26. Ames Research Staff: Equations, Tables, and Charts for Compressible Flow. NACA Rept. 1135, 1953.
27. Handbook of Supersonic Aerodynamics. NAVORD Rept. 1488, Vol. 2, Oct. 1950.
28. Foa, J. V.: Mach Number Functions for Ideal Diatomic Gases. Cornell Aeronautical Laboratory, Inc. (No. Rept. No.), Oct. 1949.
29. Kennedy, E. C.: New Mach Number Tables for Ram-Jet Flow Analysis. $\gamma = 7/5$ and $\gamma = 9/7$. Ordnance Aerophysics Laboratory OAL Memorandum 50-1. CF-1798-A. Aug. 2, 1955.
30. Henry, John R., and Bennett, J. Buel: Method for Calculation of Ram-Jet Performance. NACA TN 2357. June 1951.
31. Liepmann, H. W., and Roshko, A.: Elements of Gasdynamics. John Wiley, 1957, pp. 284-300.
32. Cronvich, Lester L.: Numerical-Graphical Methods of Characteristics for Plane Potential Shock-Free Flow Problems. Jour. of Aero. Sciences, Vol. 14, No. 4, April 1947, pp. 237-241.

33. Love, Eugene S., and Grigsby, Carl E.: Some Studies of Axisymmetric Free Jets Exhausting from Sonic and Supersonic Nozzles into Still Air and into Supersonic Streams. NACA RM L54L31, May 1955.
34. Pack, D. C.: On the Formation of Shock Waves in Supersonic Gas Jets. Quarterly Jour. of Mech. and Appl. Math., Vol. I, Pt. 1, March 1948, pp. 1-17.
35. Rousso, Morris D., and Baughman, L. Eugene: Spreading Characteristics of a Jet Expanding from Choked Nozzles at Mach 1.91. NACA TN 3836, December 1956.

TABLE I

CHARACTERISTIC CONSTANTS FOR THE DOWNSTREAM FLOW FIELD AT
 CRITICAL HEAT ADDITION FOR $M_0 = 2.0$ AND 6.0^*

Characteristics in the region between the wall and the inter-
 face.

$$M_0 = 2.0: \quad \gamma_R + \theta_R = \gamma_L - \theta_L = 0, 0.089, 1.937, 7.613, 18.001, \\
 18.1, 18.4, 18.5, 18.8, 18.9, \\
 18.9.$$

$$M_0 = 6.0: \quad \gamma_R + \theta_R = \gamma_L - \theta_L = 0, 0.089, 1.937, 7.613, 18.001, \\
 36.401, 36.1, 36.5, 37.9, 41.3.$$

Left-running characteristics emanating from the interface.

$$M_0 = 2.0: \quad \gamma_L - \theta_L = 8.2, 9.8.$$

$$M_0 = 6.0: \quad \gamma_L - \theta_L = 4.2, 43.2, 47.7.$$

Right-running characteristics emanating from the shock wave.

$$M_0 = 2.0: \quad \gamma_R + \theta_L = 26.2, 26.2.$$

$$M_0 = 6.0: \quad \gamma_R + \theta_L = 77.8, 78.2, 79.5.$$

* Characteristic constants, in degrees, are given in the order in which the characteristics occur as one proceeds downstream from the plane of heat addition in Figs. 16 and 17. Constants for characteristics emanating from linearly interpolated points in the shock-wave-interface region are not presented. Constants for characteristics which are dependent upon the interaction with the shock wave are specified only to one-tenth degree since the available shock wave charts could be read only to this degree of accuracy.



FIG 2.- TWO POSSIBLE WING CONFIGURATIONS TO WHICH THE ANALYSIS IS APPLICABLE.

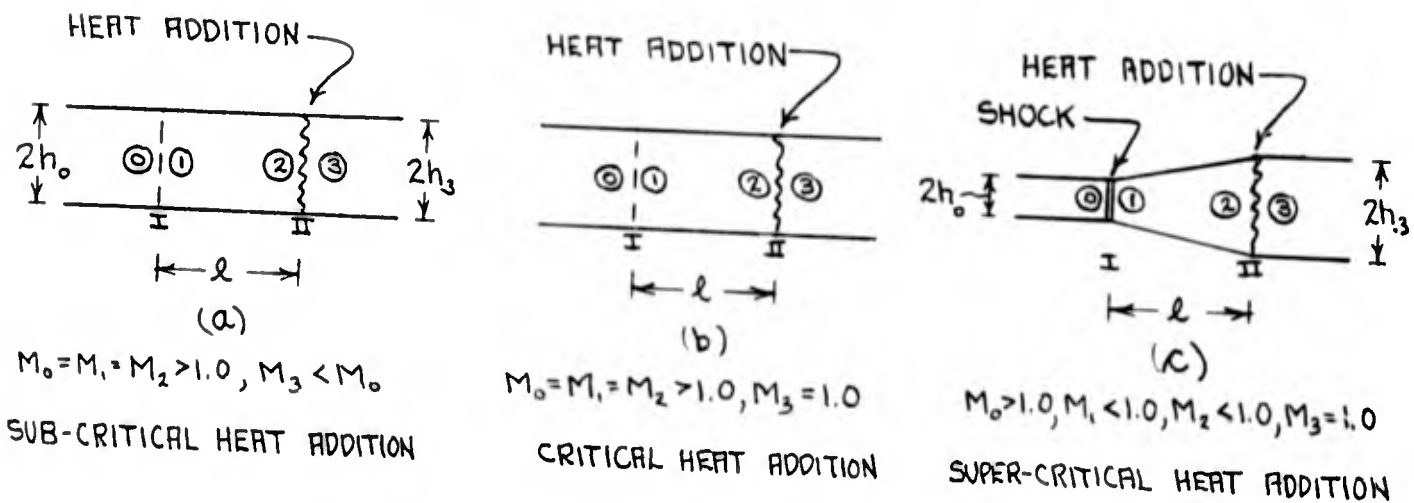


FIG 3.- ONE-DIMENSIONAL FLOW WITH HEAT ADDITION IN A VARIABLE AREA DUCT WITH A FIXED MACH NUMBER, M_0 , FAR UPSTREAM.

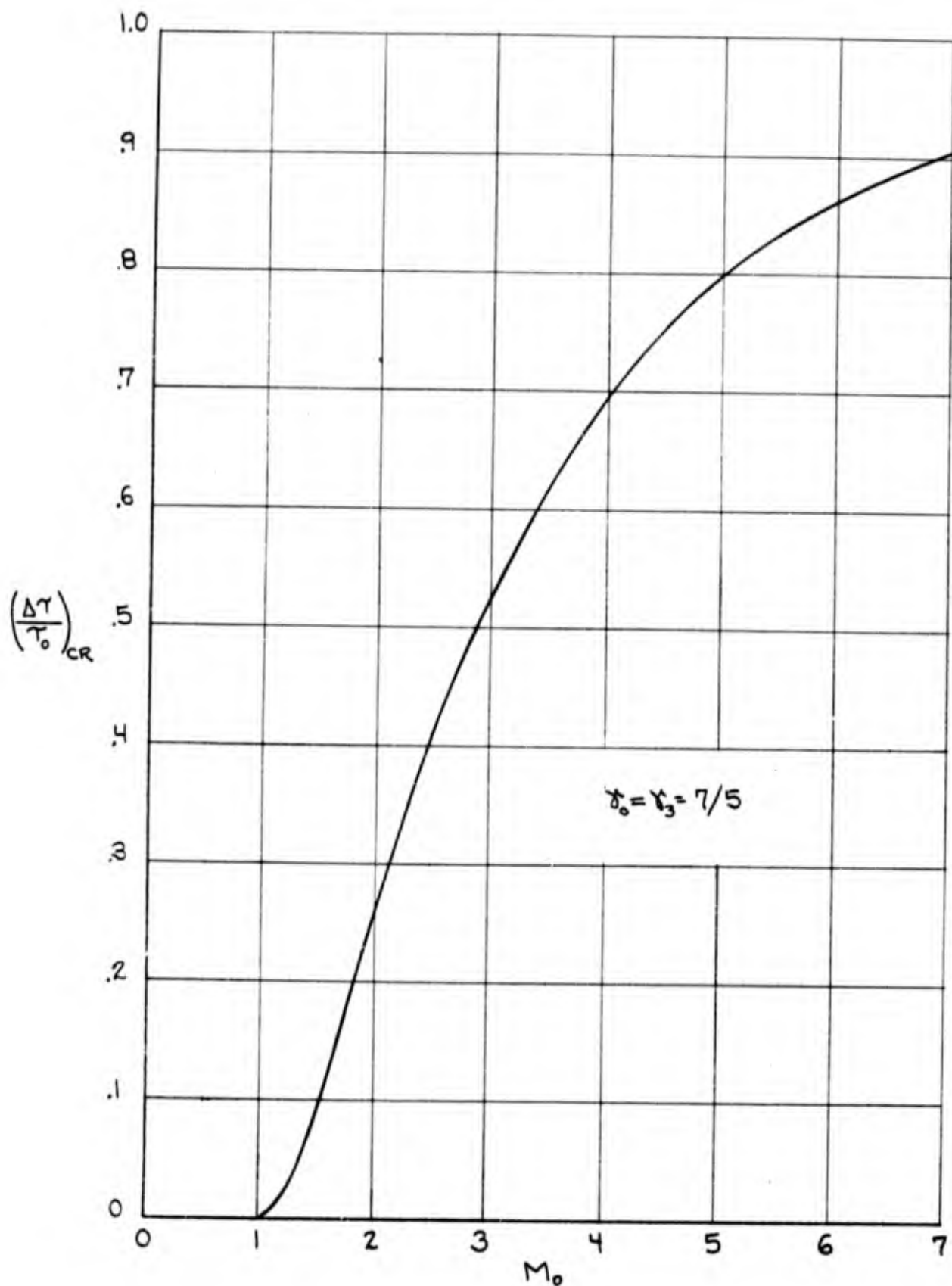


FIG 4.- TOTAL-TEMPERATURE RISE AS A FUNCTION OF FREE-STREAM MACH NUMBER AT CRITICAL HEAT ADDITION.

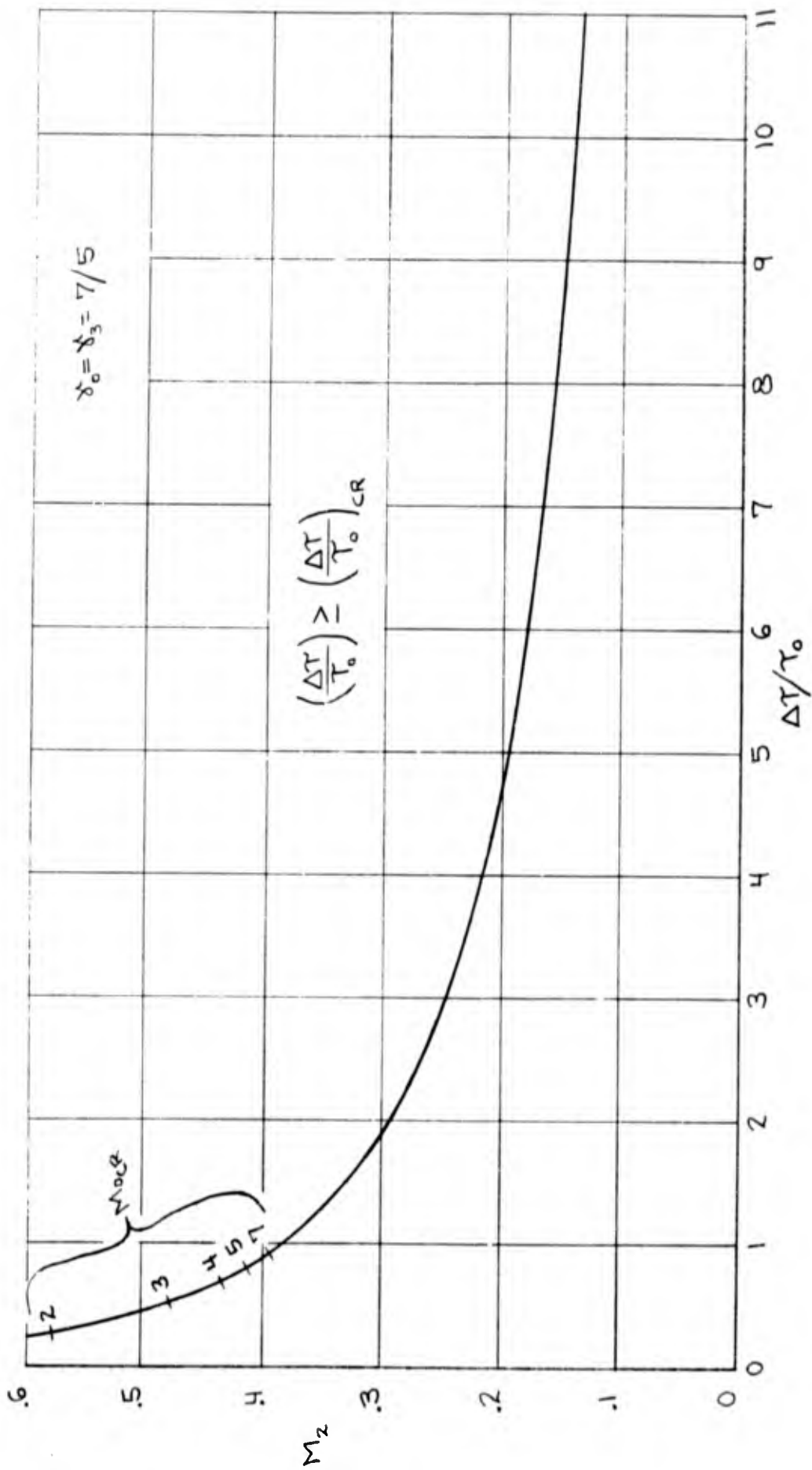


FIG 5.-MACH NUMBER AHEAD OF THE PLANE OF HEAT ADDITION AS A FUNCTION OF TOTAL-TEMPERATURE INCREASE FOR FLOW WITH SUPER-CRITICAL HEAT ADDITION AT CONSTANT AREA IN A VARIABLE AREA DUCT WITH A FIXED UPSTREAM MACH NUMBER, M_0 .

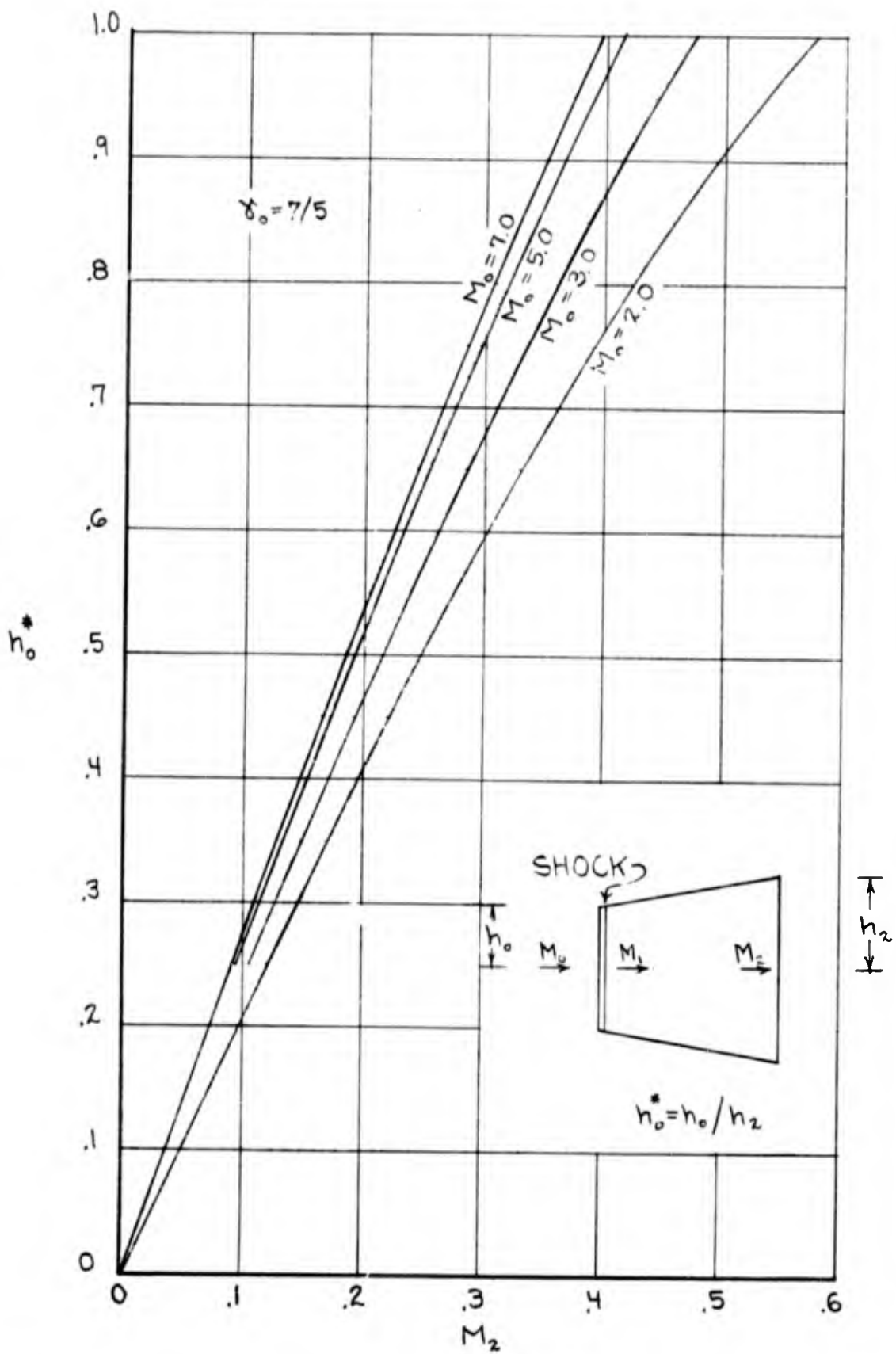


FIG 6.-ENTRANCE TO EXIT AREA RATIO AS A FUNCTION OF EXIT AND ENTRANCE MACH NUMBERS FOR A STREAM TUBE WITH SHOCK AT ENTRANCE.

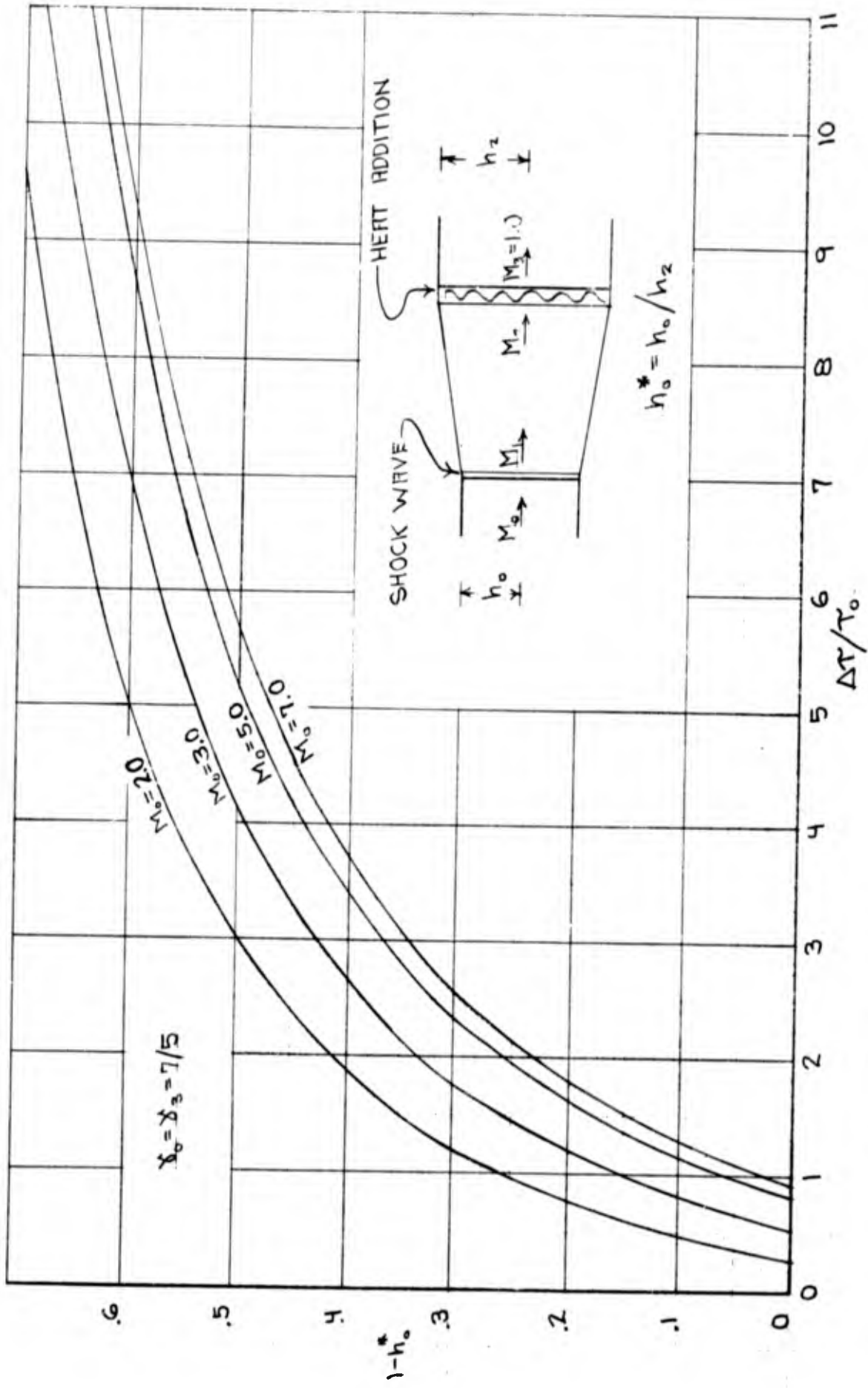


FIG 7.-SPILLAGE, $1-h_0^*$, AS A FUNCTION OF TOTAL-TEMPERATURE INCREASE AND FREE-STREAM MACH NUMBER.

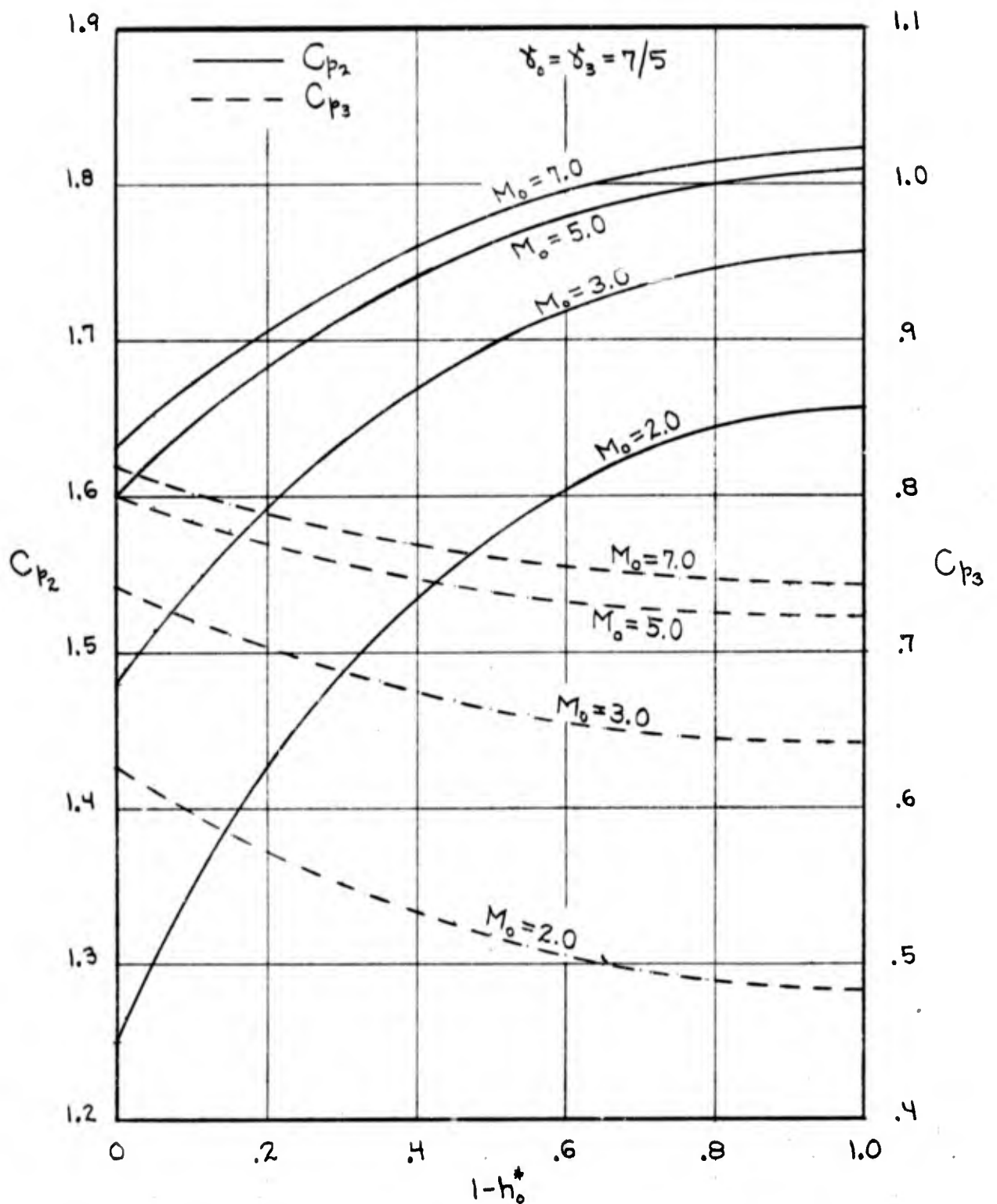


FIG 8 .-PRESSURE COEFFICIENTS FORWARD AND AFT OF THE HEATER AS A FUNCTION OF SPILLAGE AND FREE-STREAM MACH NUMBER.

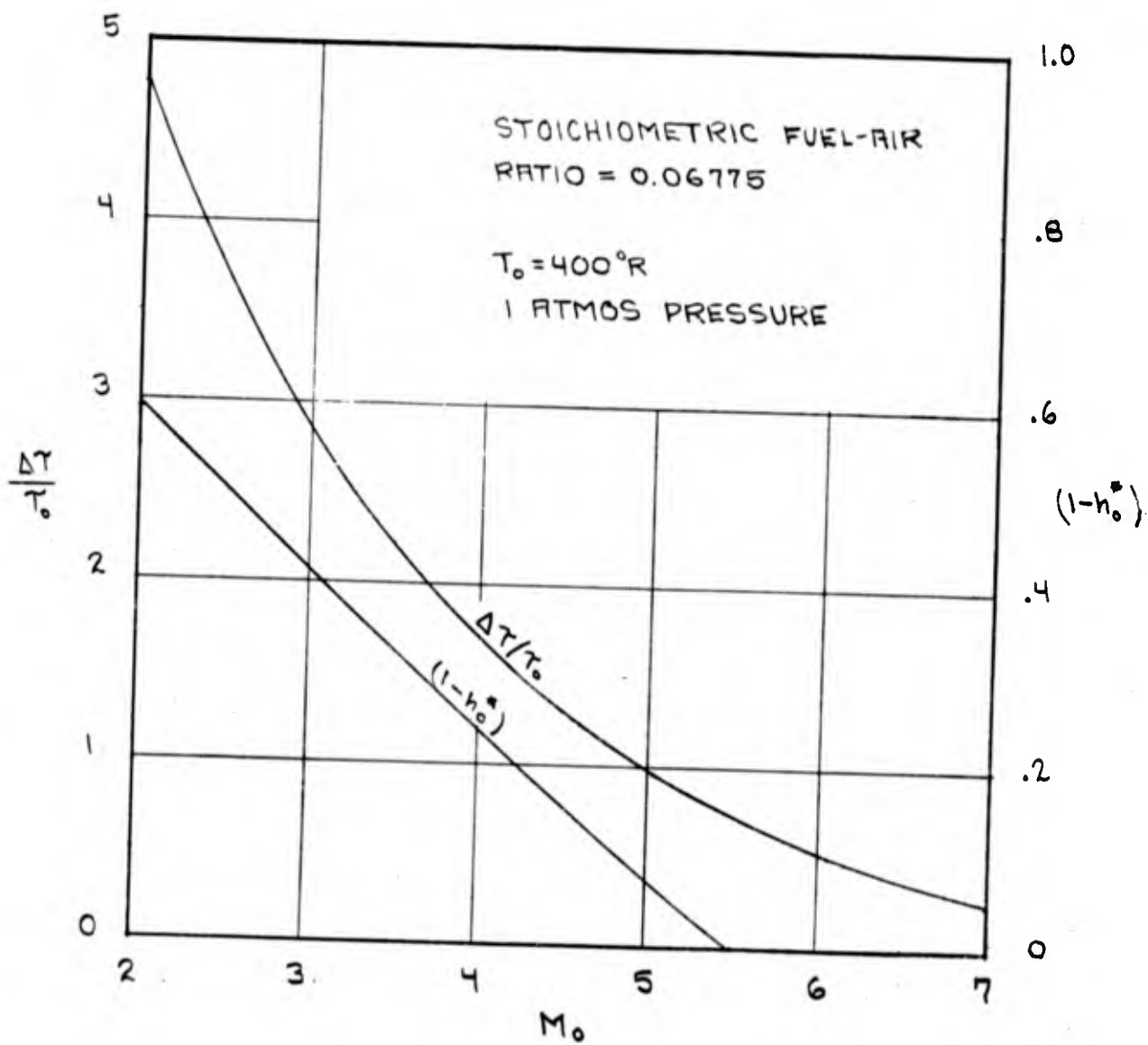


FIG 9 - TOTAL-TEMPERATURE INCREASE AND THE CORRESPONDING SPILLAGE FOR CONSTANT-PRESSURE COMBUSTION OF A STOICHIOMETRIC MIXTURE OF KEROSENE AND AIR AT INITIAL VALUES OF T_0 CORRESPONDING TO M_0 AND T_0 .

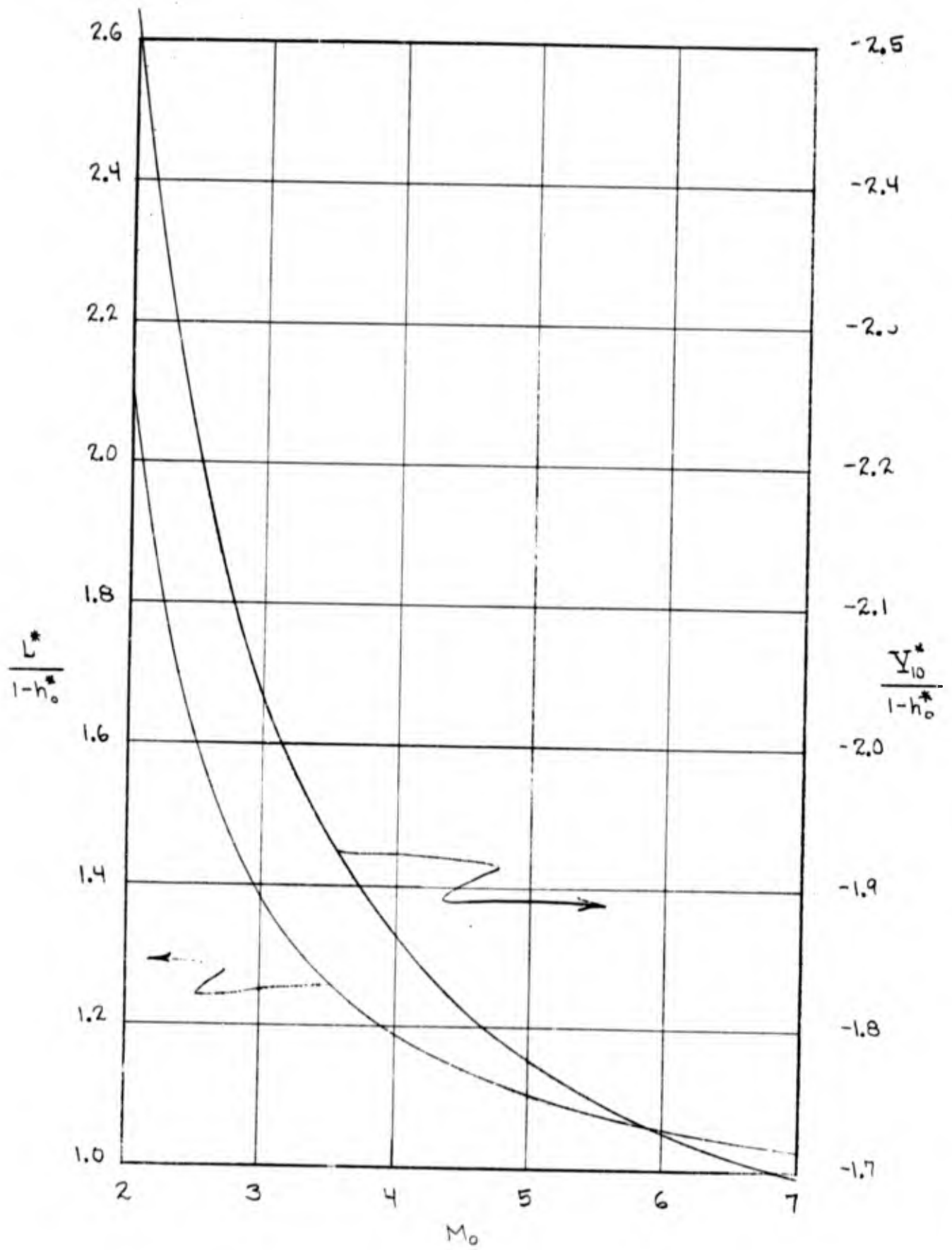


FIG 10.-SHOCK-STANDOFF DISTANCE AND FORWARD NORMAL-FORCE COEFFICIENT AS A FUNCTION OF SPILLAGE AND FREE-STREAM MACH NUMBER.

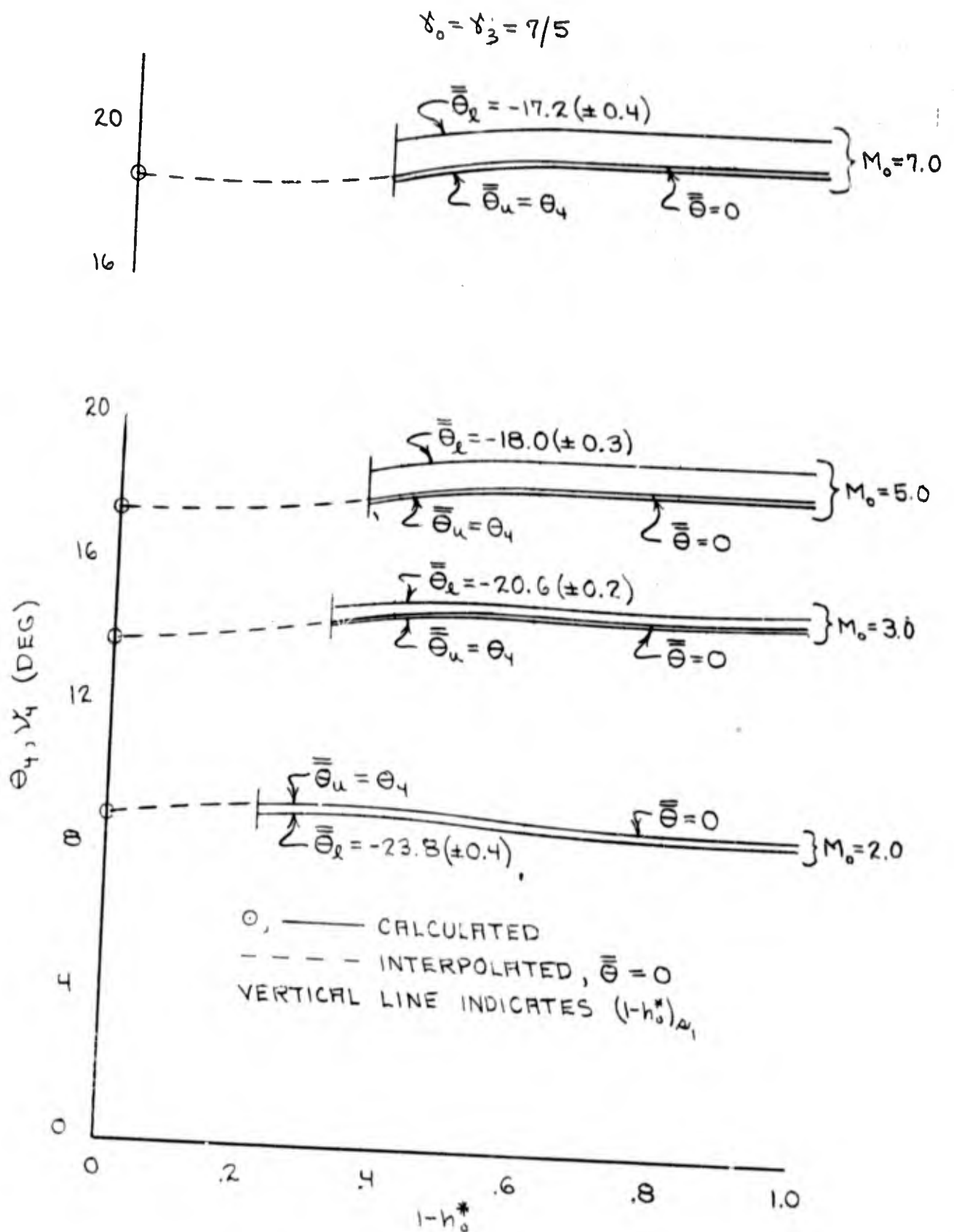


FIG. 11.-THE EFFECT OF THE UPPER AND LOWER LIMITING VALUES OF $\bar{\theta}$ UPON θ_4 IN THE RESTRICTED METHOD. REPRESENTATIVE VALUES OF $\bar{\theta}_c$, AND THEIR POSSIBLE DEVIATIONS IN THE RESTRICTED SPILLAGE RANGE, ARE GIVEN ON EACH LOWER LIMIT CURVE.

$$\delta_0 = \delta_3 = 7/5$$

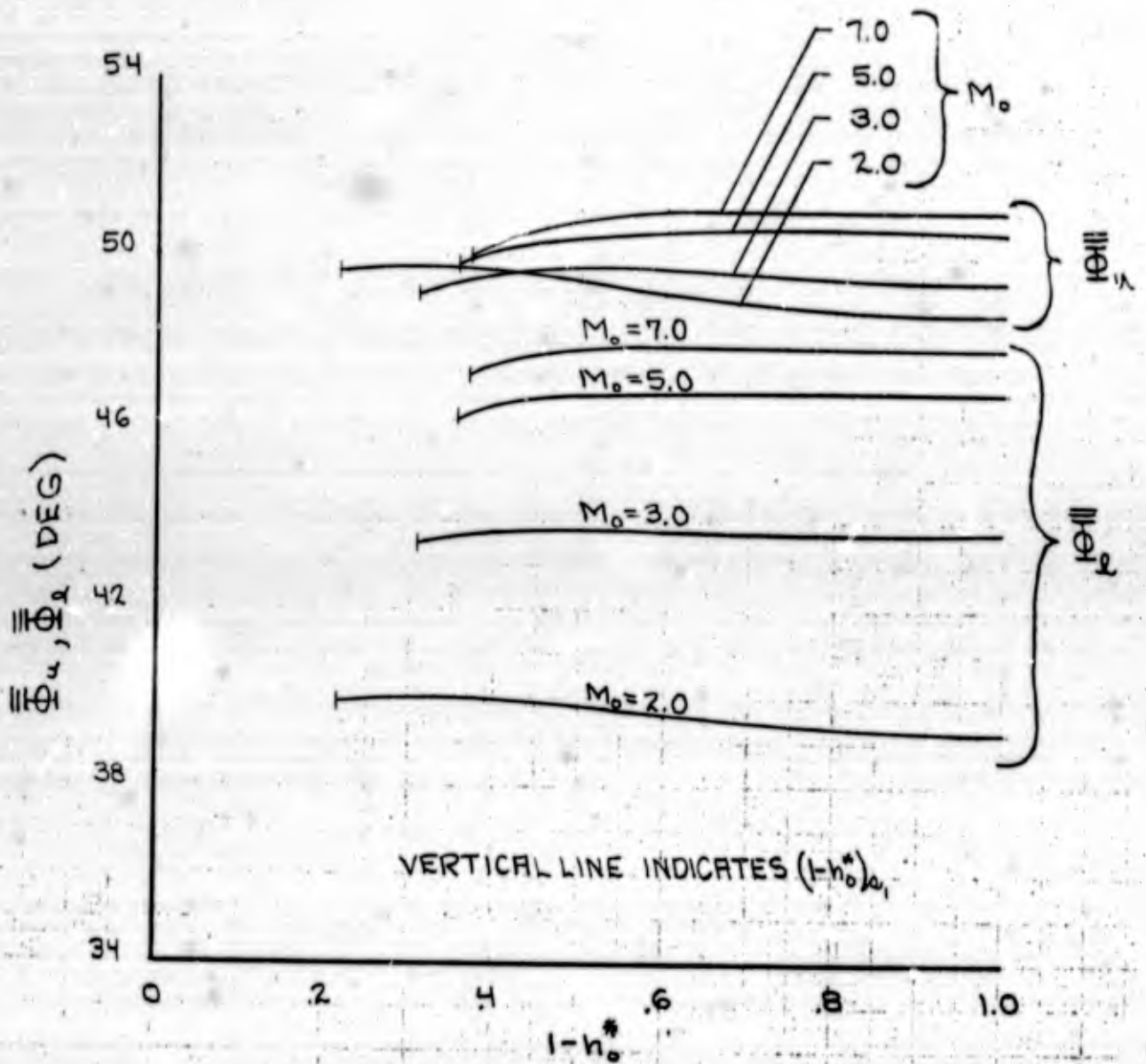


FIG 12.-THE MEAN SECOND-SHOCK ANGLES CORRESPONDING TO THE UPPER AND LOWER LIMITING VALUES OF $\bar{\theta}$ IN THE RESTRICTED METHOD.

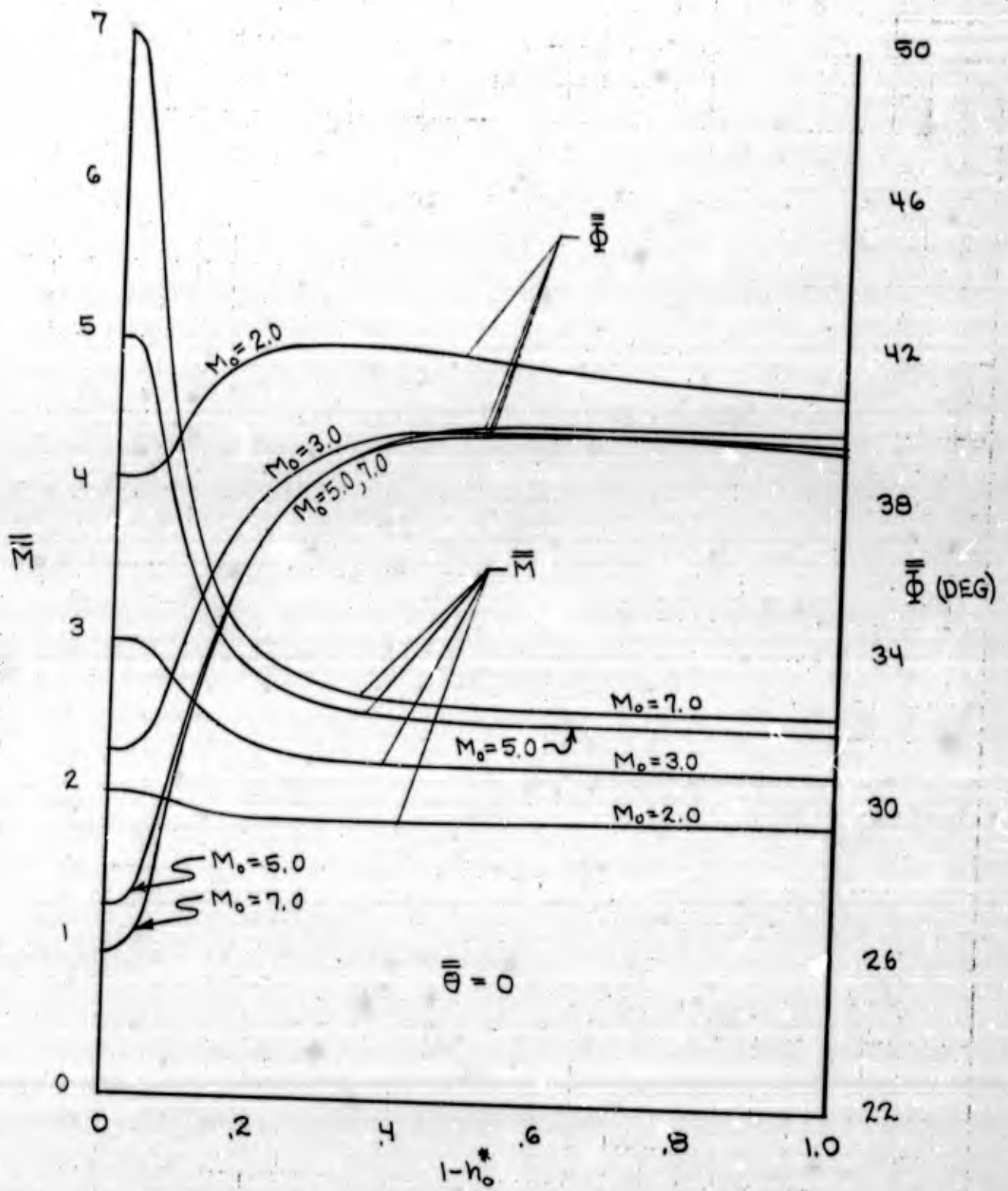


FIG. 13.- THE MEAN MACH NUMBER \bar{M} AND THE MEAN SECOND-SHOCK ANGLE $\bar{\Phi}$ AS A FUNCTION OF SPILLAGE AND FREE-STREAM MACH NUMBER AS OBTAINED BY THE FINAL METHOD.

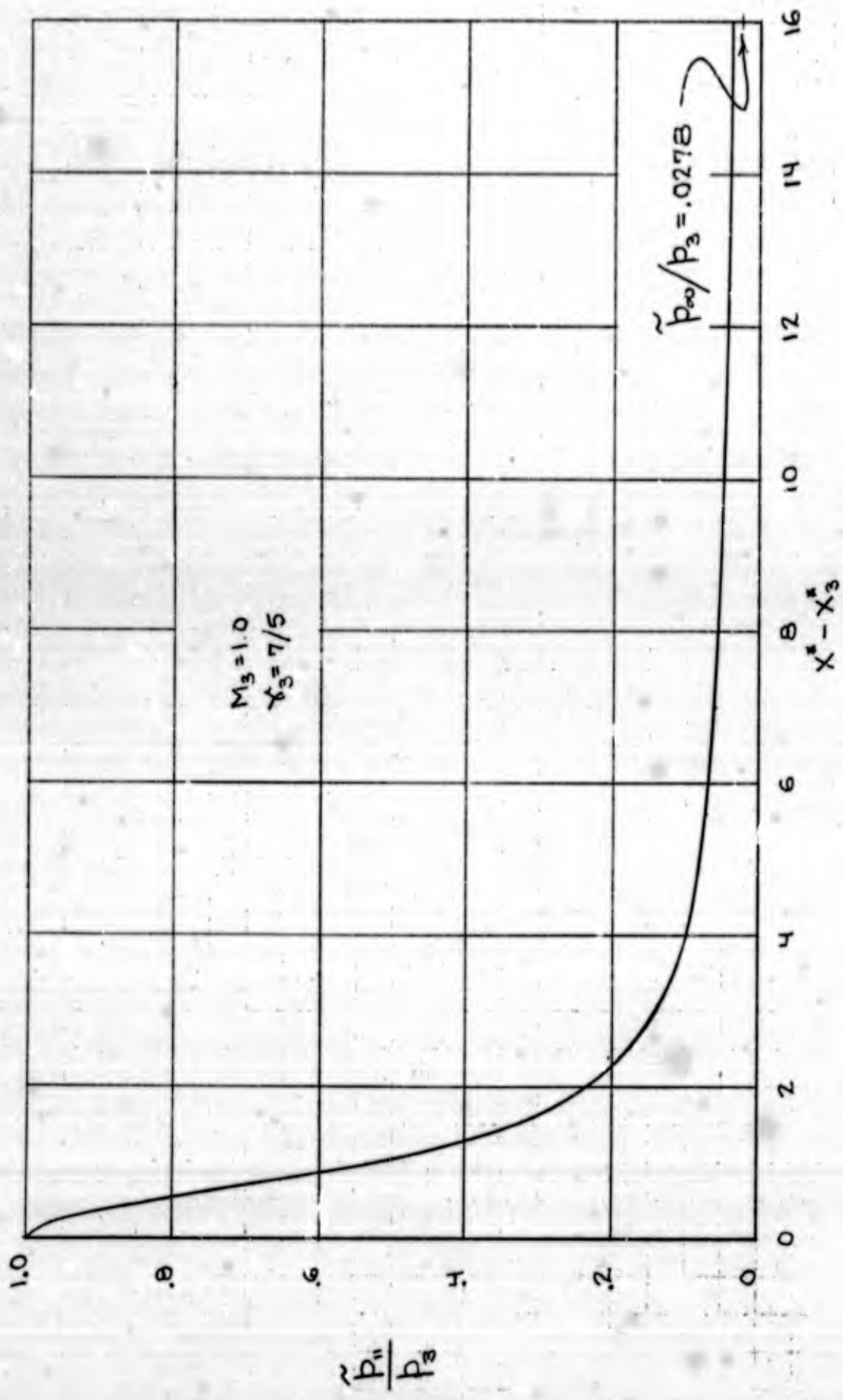


FIG 14.-THE DOWNSTREAM WALL-PRESSURE DISTRIBUTION FOR A SIMPLY REFLECTED PRANDTL-MEYER EXPANSION.

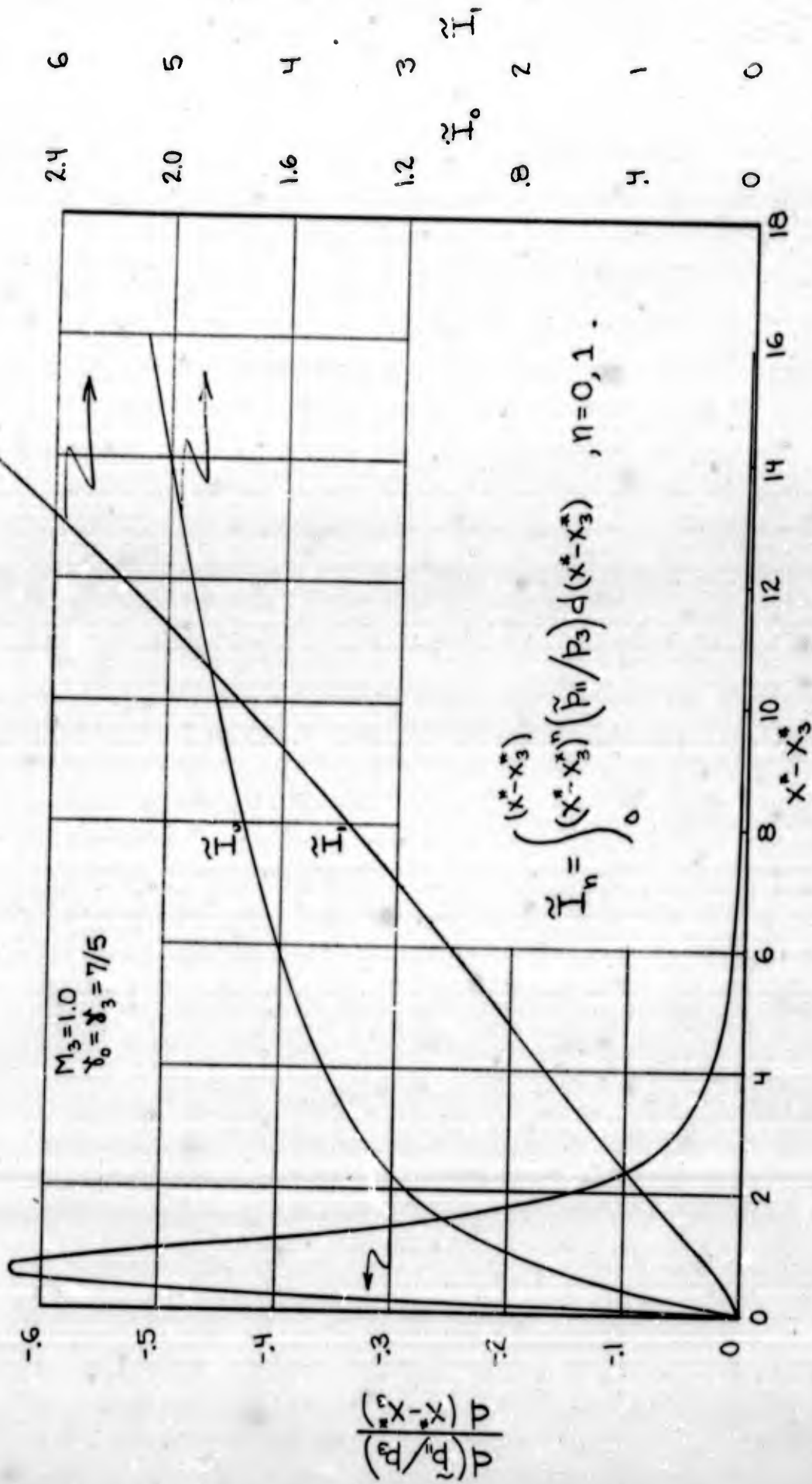


FIG 15.- SOME PROPERTIES OF THE DOWNSTREAM WALL-PRESSURE DISTRIBUTION FOR A SIMPLY REFLECTED PRANDTL-MEYER EXPANSION.

$P_3/P_0 = 5.22$ $P_3/P_0 = 2.75$

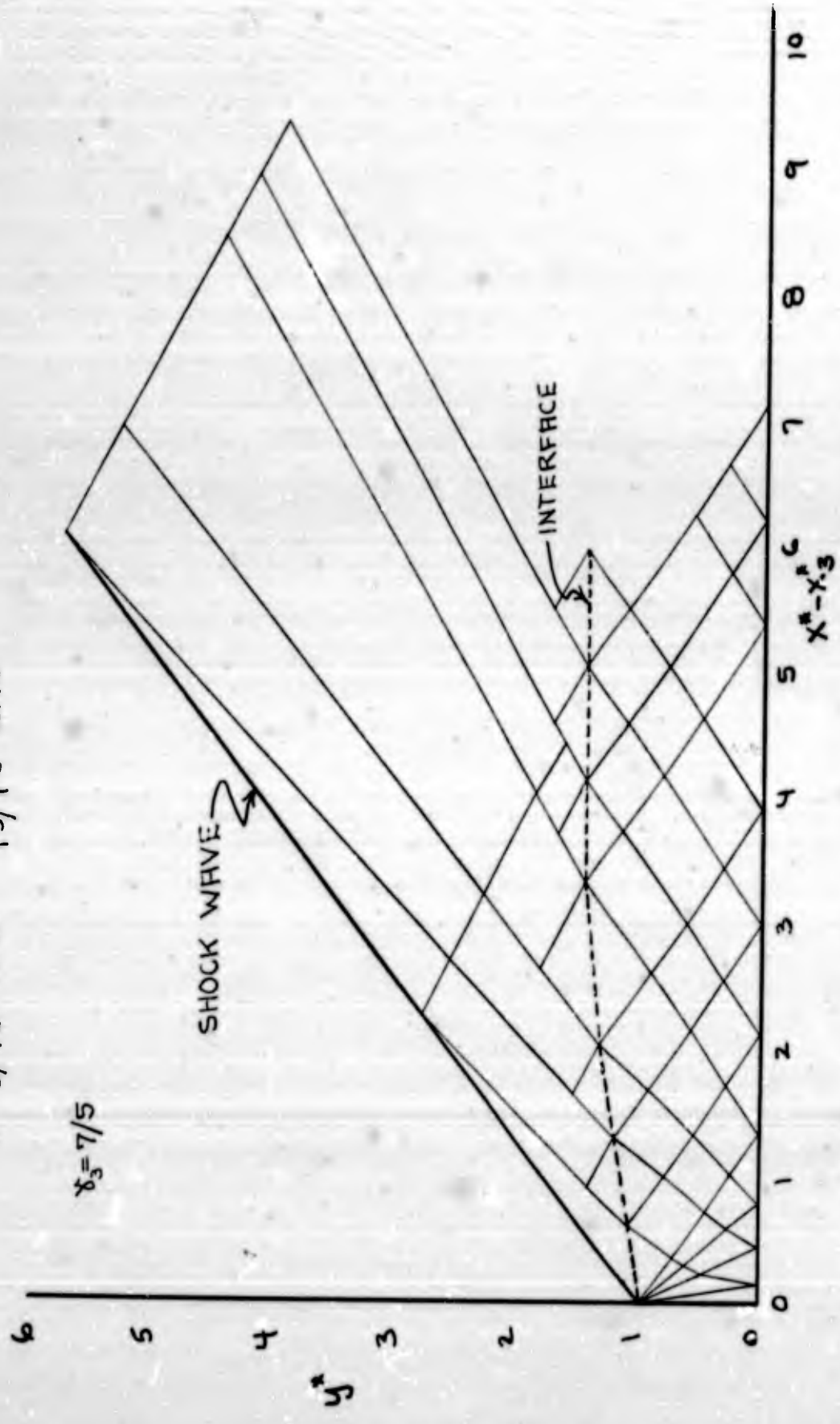


FIG 16.- DOWNSTREAM CHARACTERISTICS DIAGRAM FOR CRITICAL-HEAT-ADDITION FLOW AT $M_0 = 2.0$.

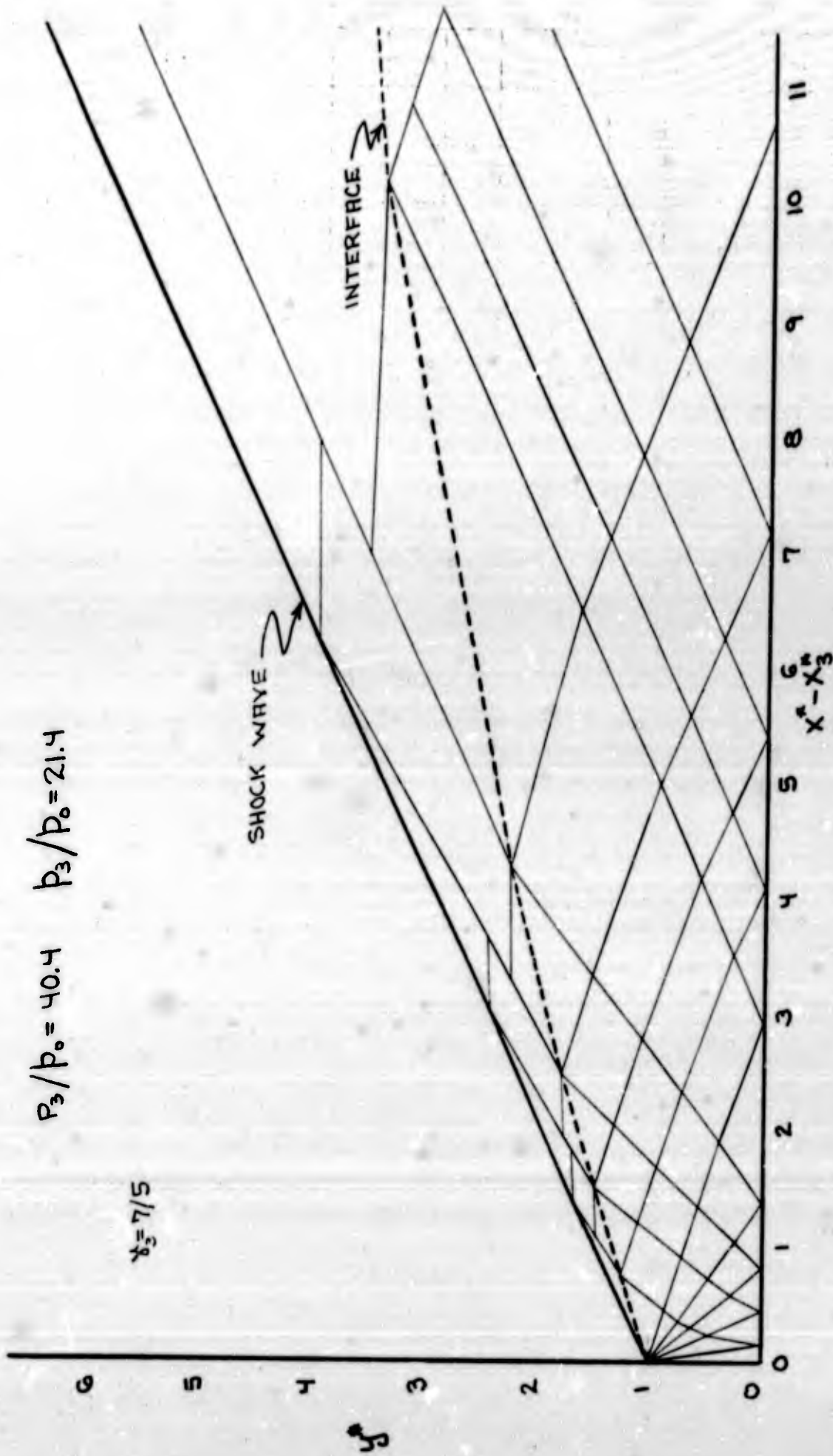


FIG 17.- DOWNSTREAM CHARACTERISTICS DIAGRAM FOR CRITICAL-HEAT-ADDITION
FLOW AT $M_0=6.0$.

$$\gamma_0 = \gamma_3 = \gamma/5$$

$M_0 = 2.0$	$M_0 = 6.0$	METHOD OF CHARACTERISTICS SOLUTION	
0	Δ	APPROXIMATE METHOD OF THIS PAPER	
0.3636	0.0468	P_0/P_3	

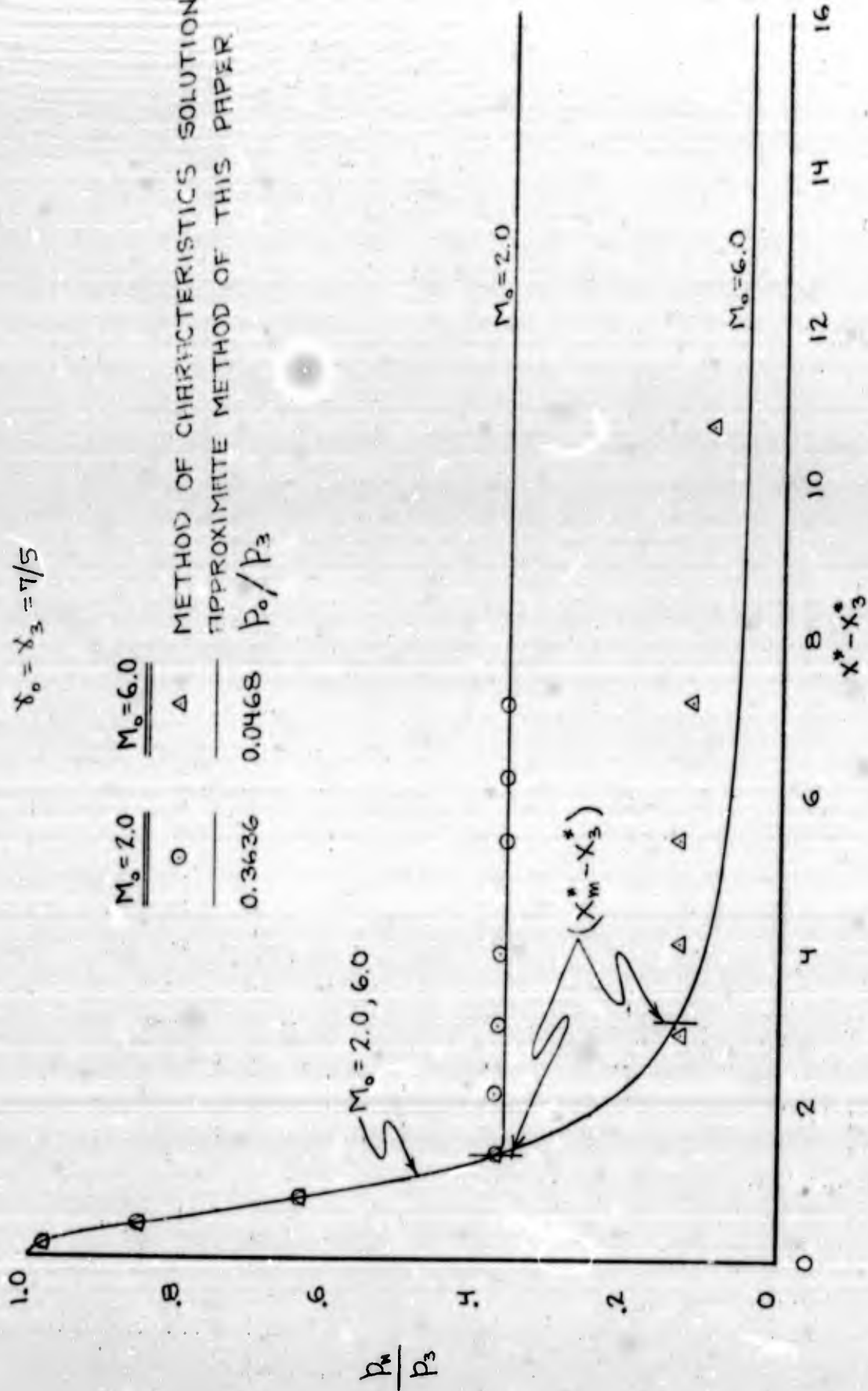


FIG 18.-COMPARISON OF THE APPROXIMATE AND EXACT DOWNSTREAM WALL-PRESSURE DISTRIBUTION FOR: CRITICAL-HEAT-ADDITION FLOW AT $M_0 = 2.0$ AND $M_0 = 6.0$.

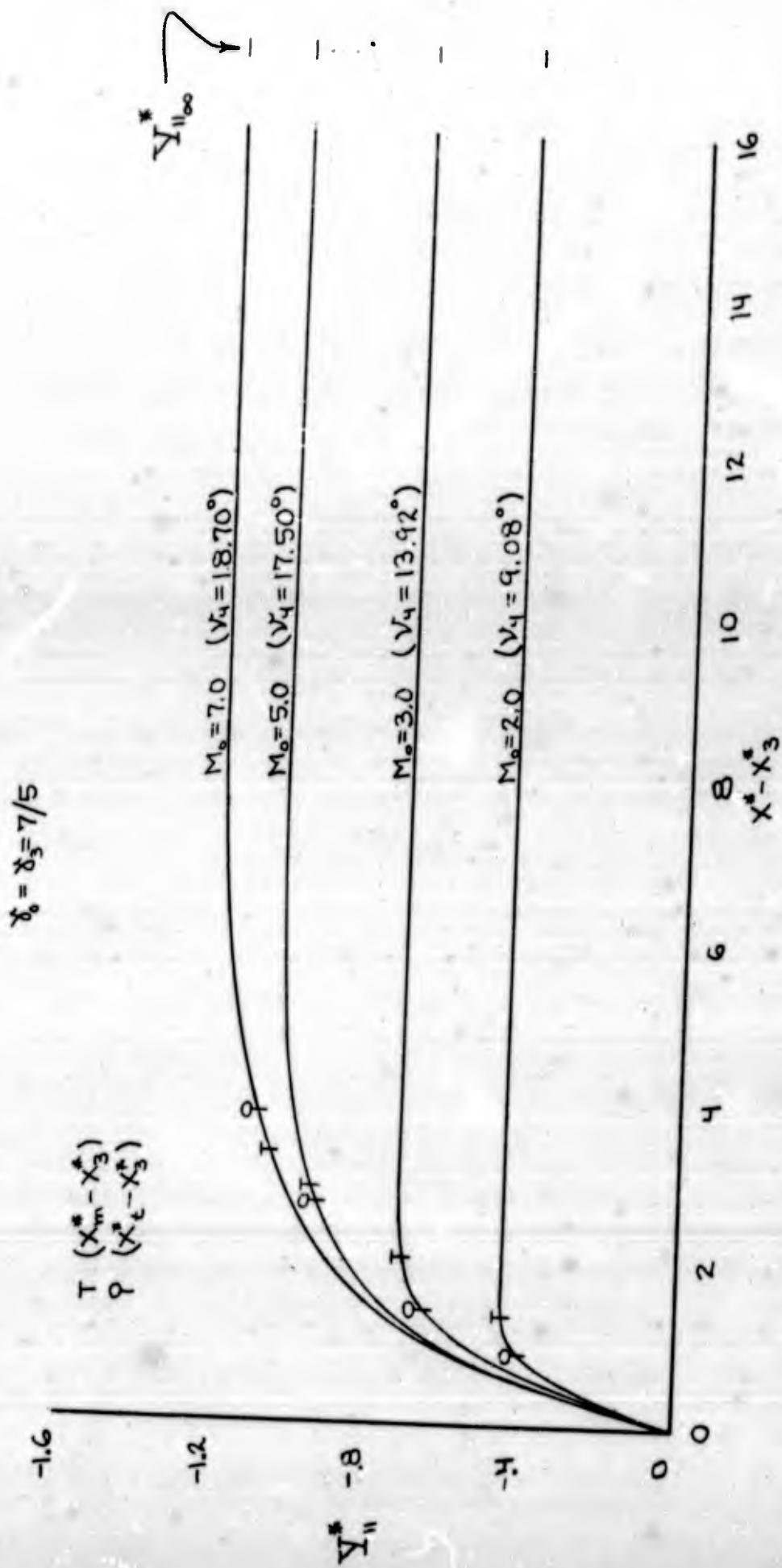


FIG 19.-CUMULATIVE RIFT NORMAL-FORCE COEFFICIENT AS A FUNCTION OF DOWNSTREAM POSITION AND FREE-STREAM MACH NUMBER FOR ZERO SPILLAGE.

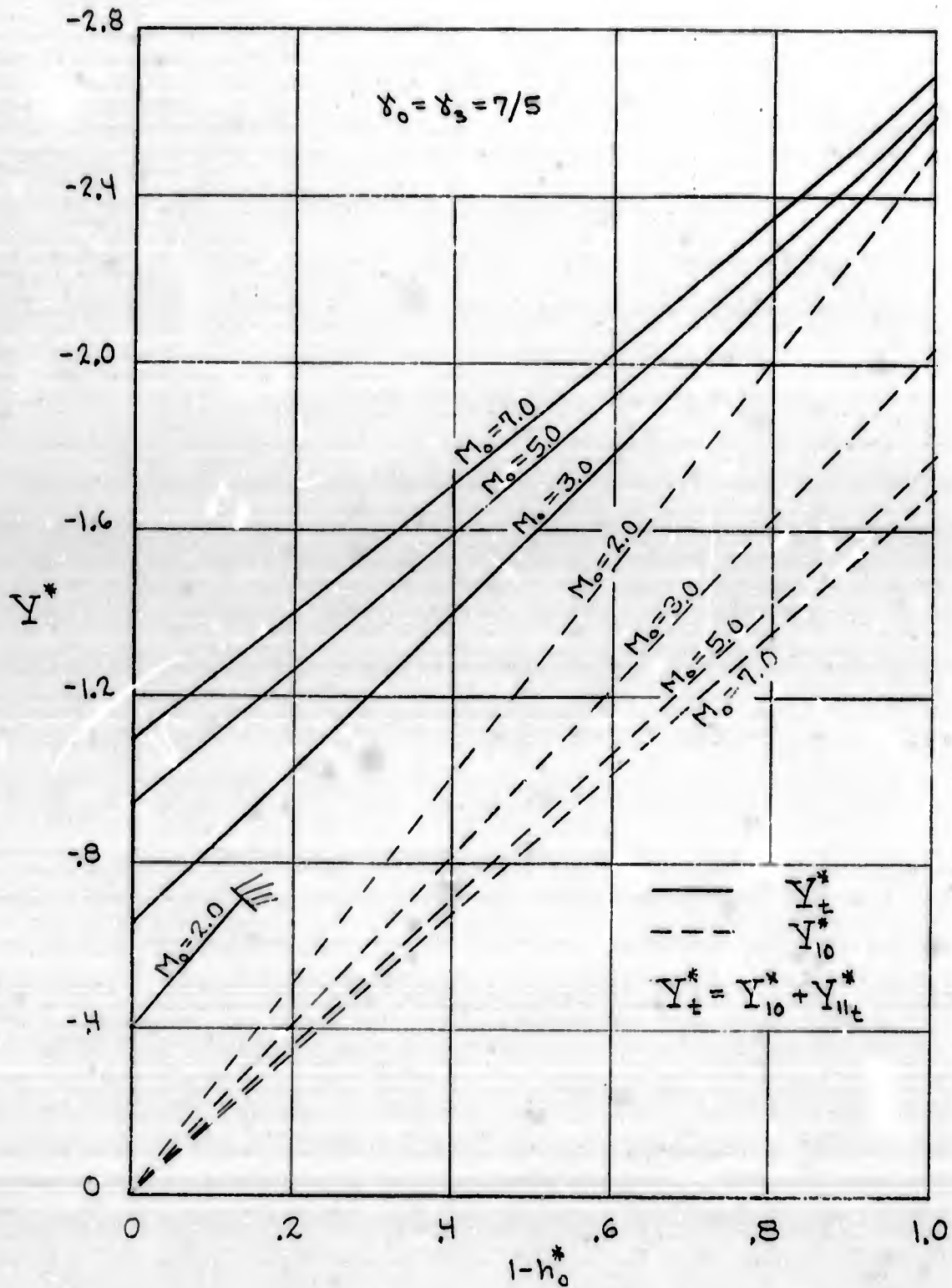


FIG 20.-THE FORWARD NORMAL-FORCE COEFFICIENT Y_{10}^* AND THE TOTAL NORMAL-FORCE COEFFICIENT Y_t^* AS FUNCTIONS OF SPILLAGE AND FREE-STREAM MACH NUMBER.

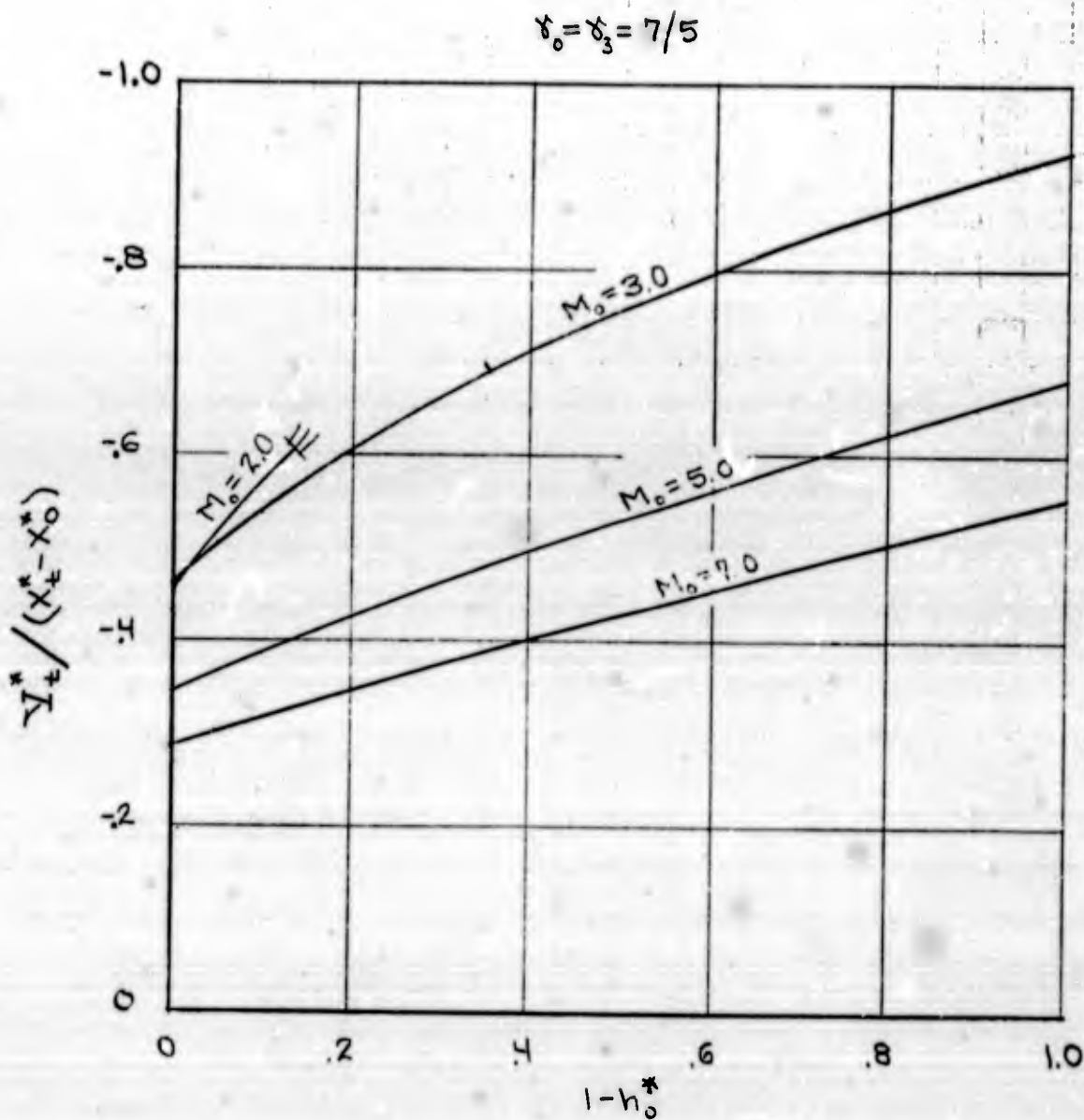


FIG 21.-THE AVERAGE NORMAL FORCE PER UNIT LENGTH FOR A FLAT PLATE TERMINATED AT X_+^* AS A FUNCTION OF SPILLAGE AND FREE-STREAM MACH NUMBER.

$$\gamma_0 = \gamma_3 = 7/5$$

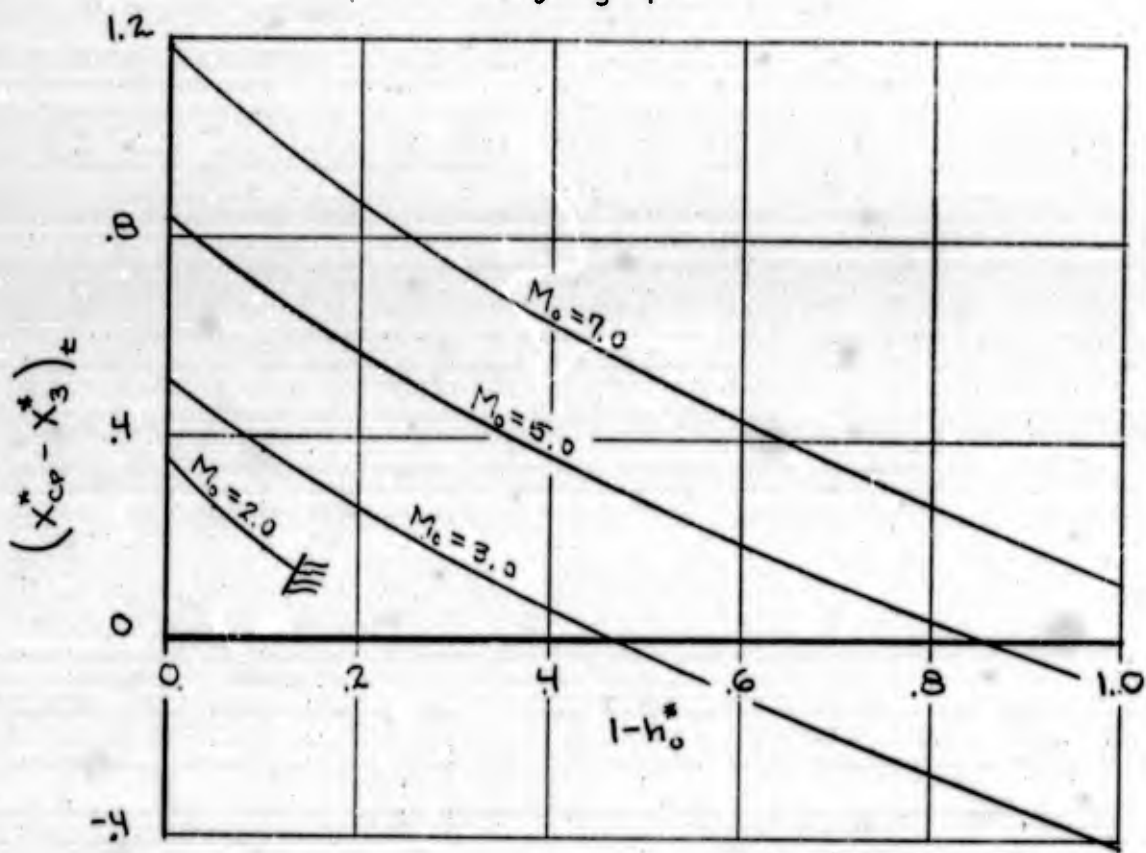


FIG 22.-THE CENTER OF PRESSURE OF A FLAT PLATE TERMINATED AT X_3^* AS A FUNCTION OF SPILLAGE AND FREE-STREAM MACH NUMBER.

$$\gamma_0 = \gamma_3 = 7/5$$

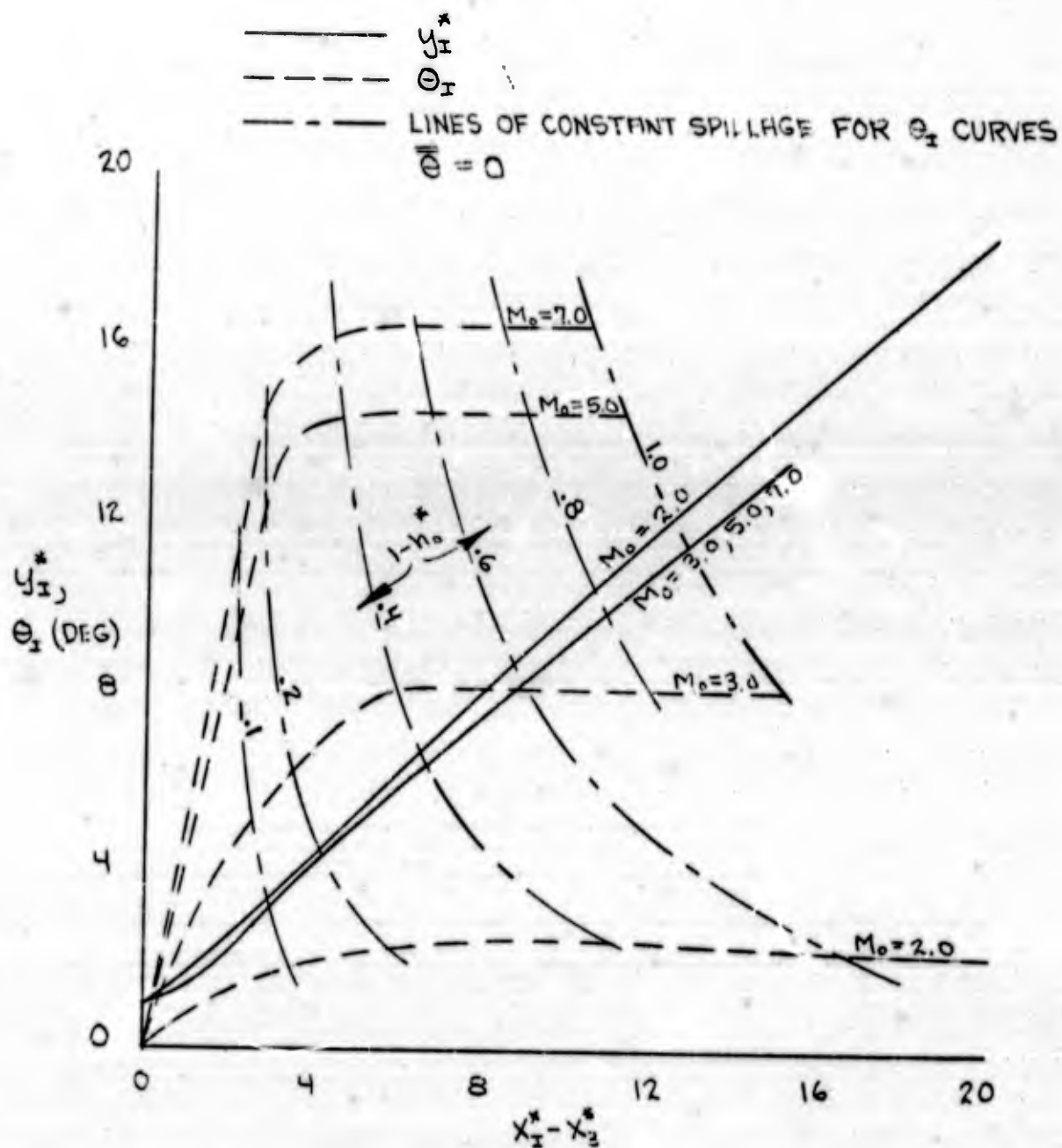


FIG 23.- COORDINATES OF THE INTERSECTION OF THE FIRST AND SECOND SHOCK WAVES, AND THE FLOW DIRECTION θ_I AFT OF THE FIRST SHOCK WAVE (NEGLECTING INTERACTION) AT THE POINT OF INTERSECTION.